MCB
Journals.ASM.org

Transient Receptor Potential Channel 1 Deficiency Impairs Host Defense and Proinflammatory Responses to Bacterial Infection by Regulating Protein Kinase Cα Signaling

Xikun Zhou,[a,b] Yan Ye,[b] Yuyang Sun,[b] Xuefeng Li,[a,b] Wenxue Wang,[b] Breanna Privratsky,[b] Shirui Tan,[b] Zongguang Zhou,[c] Canhua Huang,[a] Yu-Quan Wei,[a] Lutz Birnbaumer,[d] Brij B. Singh,[b] Min Wu[b]

State Key Laboratory of Biotherapy/Collaborative Innovation Center for Biotherapy, West China Hospital, Sichuan University, Chengdu, China[a]; Department of Basic Sciences, University of North Dakota, Grand Forks, North Dakota, USA[b]; Department of Gastrointestinal Surgery, West China Hospital, Sichuan University, Chengdu, China[c]; Laboratory of Neuroscience, NIEHS, NIH, Research Triangle Park, North Carolina, USA[d]

Transient receptor potential channel 1 (TRPC1) is a nonselective cation channel that is required for Ca^{2+} homeostasis necessary for cellular functions. However, whether TRPC1 is involved in infectious disease remains unknown. Here, we report a novel function for TRPC1 in host defense against Gram-negative bacteria. TRPC1$^{-/-}$ mice exhibited decreased survival, severe lung injury, and systemic bacterial dissemination upon infection. Furthermore, silencing of TRPC1 showed decreased Ca^{2+} entry, reduced proinflammatory cytokines, and lowered bacterial clearance. Importantly, TRPC1 functioned as an endogenous Ca^{2+} entry channel critical for proinflammatory cytokine production in both alveolar macrophages and epithelial cells. We further identified that bacterium-mediated activation of TRPC1 was dependent on Toll-like receptor 4 (TLR4), which induced endoplasmic reticulum (ER) store depletion. After activation of phospholipase Cγ (PLC-γ), TRPC1 mediated Ca^{2+} entry and triggered protein kinase Cα (PKCα) activity to facilitate nuclear translocation of NF-κB/Jun N-terminal protein kinase (JNK) and augment the proinflammatory response, leading to tissue damage and eventually mortality. These findings reveal that TRPC1 is required for host defense against bacterial infections through the TLR4-TRPC1-PKCα signaling circuit.

Pseudomonas aeruginosa and *Klebsiella pneumoniae* are opportunistic Gram-negative bacteria that infect a broad range of individuals, particularly immunocompromised people, causing high morbidity and mortality. These bacteria are increasingly becoming resistant to almost all the conventional antibiotics and remain major health threats (1, 2). Better understanding of the mechanism of host-pathogen interaction may facilitate the development of novel approaches to treat these infections. A number of studies have thus far focused on the pathogenesis of *P. aeruginosa* and *K. pneumoniae* in airway infectious diseases and have identified some critical innate immunity regulators for early-stage host defense (3–5).

Members of the transient receptor potential channel (TRPC) and Orai families have been suggested as mediators of Ca^{2+} entry channels in nonexcitable cells (6). Activation of the phospholipase C (PLC) signaling pathway generates inositol trisphosphate (IP_3) and diacylglycerol (DAG), which initiates Ca^{2+} release from the endoplasmic reticulum (ER) stores followed by the activation of Ca^{2+} entry channels that increase cytosolic Ca^{2+} levels (7, 8). Ca^{2+} entry through receptor-mediated channels is essential for regulating cellular functions, and TRPC1, which functions as a nonselective cation channel in many cell types, has been shown to be important in Ca^{2+} entry that is initiated by store depletion (7, 9). In particular, TRPC1 is reportedly associated with cell proliferation, cell migration, enzyme and fluid secretion, normal metabolism in various organ systems, and cancer metastasis (6, 10, 11). TRPC1 could also form a heteromultimer with Orai1 and stromal interaction molecule 1 (STIM1), which are essential for Ca^{2+} signaling (12–14). This interaction may allow the activation of immune ligands (e.g., Toll-like receptors [TLRs]), and thus TRPC channel proteins may play a role in host defense, which has been demonstrated only in the context of lipopolysaccharide (LPS) by regulating cytokine production and inflammatory response. Although TRPC1 is reportedly involved in LPS-induced sepsis models (15), its role in whole-microorganism infections has not been investigated.

Here, we set out to characterize the role of TRPC1 in infection of whole *P. aeruginosa* and *K. pneumoniae* bacteria and the potential molecular mechanism using both mouse and cell culture models. We report for the first time that TRPC1 and its associated endogenous Ca^{2+} channel participate in cytokine production in both lung alveolar macrophages and epithelial cells. The Ca^{2+} entry via TRPC1 positively modulates inflammatory responses, as TRPC1 deficiency results in decreased Ca^{2+} entry and increased infection susceptibility. After PLC-γ activation, TLR4-mediated TRPC1 induces protein kinase Cα (PKCα) phosphorylation, which in turn induces Jun N-terminal protein kinase (JNK)/

Received 9 March 2015 **Returned for modification** 14 April 2015
Accepted 19 May 2015

Accepted manuscript posted online 1 June 2015

Citation Zhou X, Ye Y, Sun Y, Li X, Wang W, Privratsky B, Tan S, Zhou Z, Huang C, Wei Y-Q, Birnbaumer L, Singh BB, Wu M. 2015. Transient receptor potential channel 1 deficiency impairs host defense and proinflammatory responses to bacterial infection by regulating protein kinase Cα signaling. Mol Cell Biol 35:2729–2739. doi:10.1128/MCB.00256-15.

Address correspondence to Brij B. Singh, brij.singh@med.und.edu, or Min Wu, min.wu@med.und.edu.

X.Z, Y.Y., and Y.S. contributed equally to this article.

Supplemental material for this article may be found at http://dx.doi.org/10.1128/MCB.00256-15.

doi:10.1128/MCB.00256-15

NF-κB nuclear translocation, augmenting the production of proinflammatory cytokines.

MATERIALS AND METHODS

Animals. TRPC1 knockout (KO) (TRPC1$^{-/-}$) and wild-type (WT) mice were bred at the animal facility as described in reference 16. Animals were kept in a specific-pathogen-free facility of the University of North Dakota. All animal studies were performed in accordance with the guidelines approved by the Institutional Animal Care and Use Committee (IACUC number 1204-5).

Primary cells and cell lines. Alveolar macrophages (AM) were isolated by bronchoalveolar lavage (BAL) and maintained in RPMI 1640 (Invitrogen, Grand Island, NY) supplemented with 10% fetal bovine serum (FBS). Murine MLE-12 lung type II epithelial cells were obtained from the American Type Culture Collection (Manassas, VA) and cultured according to the manufacturer's instructions.

Preparation of bacteria and infection. The *P. aeruginosa* WT strain PAO1 was kindly provided by S. Lory (Harvard University, Boston, MA) (17). The *K. pneumoniae* WT strain was kindly provided by V. Miller (Washington University, St. Louis, MO) (18). PAK and green fluorescent protein (GFP)-PAO1 were obtained from G. Pier (Channing Laboratory, Harvard Medical School, Boston, MA) (19). Another *P. aeruginosa* strain, Xen-41, expressing luciferase bioluminescence was purchased from Caliper Company (Perkin-Elmer, Hopkinton, MA). Bacteria were grown for about 16 h in LB broth at 37°C with shaking. The bacteria were pelleted by centrifugation at 5,000 × *g*. MLE-12 or MH-S cells were transfected with TRPC1, TLR2, TLR4, or PKCα small interfering RNA (siRNA) (50 nM) (Santa Cruz Biotechnology, Santa Cruz, CA) using Lipofectamine 2000 reagent (Invitrogen, Grand Island, NY) according to the manufacturer's instruction for 24 h. Cells were washed once with serum-free and antibiotic-free medium and changed to serum-free and antibiotic-free medium before infection. Cells were infected by bacteria at a multiplicity of infection (MOI) of 10:1 (bacterium/cell ratio) for 1 h. Cells were treated with various inhibitors 30 min before bacterial infection. Mice were anesthetized with 45 mg/kg ketamine and then intranasally instilled with 1×10^7 CFU of *P. aeruginosa* and 1×10^5 CFU for *K. pneumoniae* in 50 μl phosphate-buffered saline (PBS), quantified by growing bacteria on conventional agar dishes as described previously (3). Mice were monitored for symptoms and euthanized when they were moribund. Following bacterial infection, BAL was performed to isolate AM to determine cytokine levels in BAL fluid using enzyme-linked immunosorbent assay (ELISA).

Electrophysiology. For patch clamp experiments, cells seeded on coverslips were transferred to the recording chamber and perfused with an external Ringer solution with the following composition (millimolar): NaCl, 145; CsCl, 5; $MgCl_2$, 1; $CaCl_2$, 1; HEPES, 10; and glucose, 10 (pH 7.4 [NaOH]). All electrophysiological experiments were performed using a previously described protocol (20, 21). Briefly, whole-cell currents were recorded using an Axopatch 200B (Axon Instruments, Inc.). The patch pipette had resistances between 3 and 5 MΩ after filling with the standard intracellular solution containing the following (millimolar): cesium methane sulfonate, 150; NaCl, 8; HEPES, 10; and EGTA, 10 (pH 7.2 [CsOH]). With a holding potential of 0 mV, voltage ramps ranging from −100 mV to +100 mV and with a duration of 100 ms were delivered at 2-s intervals after a whole-cell configuration was formed. Currents were recorded at 2 kHz and digitized at 5 to 8 kHz. pClamp 10.1 software was used for data acquisition and analysis. Basal leakage was subtracted from the final currents, and average currents were shown. All experiments were carried out at room temperature.

Calcium measurements. Cells were incubated with 2 μM Fura-2 (Molecular Probes) for 45 min and washed twice with Ca^{2+}-free standard external solution (SES) (10 mM HEPES, 120 mM NaCl, 5.4 mM KCl, 1 mM $MgCl_2$, 10 mM glucose, pH 7.4). For fluorescence measurements, the fluorescence intensity of Fura-2-loaded control cells was monitored with a charge coupled-device (CCD) camera-based imaging system (Compix) mounted on an Olympus XL70 inverted microscope equipped with an Olympus 40× (numerical aperture [NA], 1.3) objective. A dual-wavelength monochrometer enabled alternative excitation at 340 and 380 nm, whereas the emission fluorescence was monitored at 510 nm with an Okra Imaging camera (Hamamatsu, Japan). The images of multiple cells collected at each excitation wavelength were processed using the C imaging PCI software (Compix Inc., Cranbery, PA) to provide ratios of Fura-2 fluorescence from excitation at 340 nm to that from excitation at 380 nm (F340/F380). Fluorescence traces shown represent $[Ca^{2+}]_i$ values that are averages from at least 30 to 40 cells and are representative of results obtained in at least 3 or 4 individual experiments in the presence of LPS from *Pseudomonas aeruginosa* (100 ng/ml; Sigma-Aldrich, St. Louis, MO) or 1-oleoyl-2-acetyl-glycerol (OAG) (100 μM; Sigma-Aldrich).

Bone marrow chimera transfer. TRPC1$^{-/-}$ and WT mice which have the same genetic background were administered antibiotics via treated drinking water (250 units/ml penicillin and 250 μg/ml streptomycin) (Gibco, Grand Island, NY) beginning 1 day before irradiation and given lethal total body irradiation (800 rads); 24 h later, they were reconstituted with bone marrow cells (1×10^7) that had been harvested from the femurs of age-matched mice. Experimental transfers were as follows: WT donors into WT recipients, WT donors into TRPC1$^{-/-}$ recipients, TRPC1$^{-/-}$ donors into WT recipients, and TRPC1$^{-/-}$ donors into TRPC1$^{-/-}$ recipients. Animals were allowed to reconstitute for ~45 days, and *P. aeruginosa* infection was performed as described above.

Western blot analysis. Rabbit polyclonal anti-TRPC1 (catalog number ACC-010) and ORAI1 (catalog number ACC-060) antibodies (Abs) were purchased from Alomone Labs. Mouse monoclonal Abs against glyceraldehyde-3-phosphate dehydrogenase (GAPDH) (catalog number sc-137179), gamma interferon (IFN-γ) (catalog number sc-32813), interleukin-6 (IL-6) (catalog number sc-1265-R), phospho-p38 (catalog number SC-7973), p38 (catalog number SC-535), phospho-extracellular signal-regulated kinase (p-ERK) (catalog number SC-7383), ERK (catalog number SC-271269), and NF-κB p65 (catalog number SC-8008), rabbit polyclonal Abs against TLR4 (catalog number SC-30002), TLR2 (catalog number SC-10739), IL-12α (catalog number SC-7925), and phospho-NF-κB p65 (Ser536) (catalog number SC-330220-R), and goat polyclonal Abs against IL-1β (catalog number SC-1252), IL-4 (catalog number sc-1261), β-actin (catalog number sc-1616), and tumor necrosis factor alpha (TNF-α) (catalog number sc-1351) were obtained from Santa Cruz Biotechnology, Inc. (Santa Cruz, CA). Rabbit monoclonal Abs against phospho-PKCα (catalog number 9375), PKCα (catalog number 2056), IκB kinase β (IKKβ) (catalog number 34673), phospho-JNK (catalog number 9258), STIM1 (catalog number 4916), SECRA (catalog number 12293), and JNK (catalog number 9251) were purchased from Cell Signaling Technology (Cambridge, MA). Mouse monoclonal Abs against IP_3 receptor (IP_3R) (catalog number 610312) was purchased from BD Biosciences (San Jose, CA).The samples derived from cells and lung homogenates were lysed in radioimmunoprecipitation assay (RIPA) buffer and their protein content quantified using the Bradford method. The cell lysates were separated by SDS-PAGE on a 12% acrylamide gel. After transfer to a polyvinylidene difluoride (PVDF) membrane, this membrane was blocked with blocking buffer containing 5% dry milk and incubated with different primary and appropriate secondary antibodies. Antibody binding was revealed by using an ECL kit (Santa Cruz, CA) as described previously (22).

***In vivo* imaging.** *P. aeruginosa* strain Xen-41, expressing luciferase bioluminescence, was purchased from Caliper Company (Perkin-Elmer, Hopkinton, MA). Bacteria were grown for about 16 h in LB broth at 37°C with shaking. The bacteria were pelleted by centrifugation at 5,000 × *g*. TRPC1$^{-/-}$ mice and WT mice were intranasally challenged with 1×10^7 CFU/mouse of *P. aeruginosa* (Xen-41), anesthetized by ketamine, and then imaged under an Ivis XRII system following the user guide plus protocols provided by the company (Perkin-Elmer). The mice were then monitored up to 24 h.

Histological analysis. Lung tissues were fixed in 4% formalin for 24 h and then processed for hematoxylin and eosin (H&E) staining in AML Laboratories, Inc. (Baltimore, MD). The leukocytes were counted using the normal optical microscope. Histological analysis was performed according to previously report (23).

AM isolation. TRPC1$^{-/-}$ and WT mice ($n = 5$) were sacrificed immediately prior to lavage, and the animal fur was dampened with 70% ethanol (EtOH). The mouse tissues were dissected from the neck to expose the trachea. A small incision was made in the trachea to allow passage of a 23-gauge lavage tube into the trachea, and then a 23-gauge needle was carefully passed into the tubing. The mouse lungs are lavaged three times with 1 ml of PBS. The retained BAL fluid was centrifuged at 600 × *g* for 5 min at 4°C. The recovered supernatants were collected and assessed for cytokine concentration using ELISA, and cell pellets were resuspended in 200 μl of PBS–1% FBS. AM cells obtained from BAL fluid were seeded in 96-well plates and grown overnight.

Confocal microscopy. MLE-12 cells were transfected with TRPC1 or PKCα siRNA for 24 h, and 25 μM TRPC1 inhibitor SKF-96365, 3 μM PKCα inhibitor Go6976. 20 μM JNK inhibitor SP600125 or 50 μg/ml NF-κB peptide inhibitor SN50 (Calbiochem, Billerica, MA) was added 30 min before bacterial infection to the indicated cells. Cells were incubated with primary anti-p-NF-κB p65 and p-JNK Abs and the secondary antibodies as described in our previously report (3). DAPI (4′,6′-diamidino-2-phenylindole) (Sigma-Aldrich) was used to stain the nucleus.

Luciferase assay. Transient transfections were performed with 2 × 10^5 MLE-12 cells plated in 6-well plates by using pNFκB-luc plasmid (Promega, Madison WI) according to the manufacturer's instructions. At 24 h after transfection, the cells were infected with bacteria for 1 h. Cell lysates were subjected to luciferase activity analysis by using a dual-luciferase reporter assay system (Promega, Madison, WI).

Phagocytosis assay. Phagocytosis was performed as described previously (3) but with minor modifications. TRPC1$^{-/-}$ and WT mice ($n = 5$) were sacrificed immediately prior to lavage, and the animal fur was dampened with 70% EtOH. The mouse tissues were dissected from the neck to expose the trachea. A small incision was made in the trachea to allow passage of a 23-gauge lavage tube into the trachea, and then a 23-gauge needle was carefully passed into the tubing. The mouse lungs are lavaged three times with 1 ml of PBS. The retained BAL fluid was centrifuged at 600 × *g* for 5 min at 4°C. The recovered supernatants were collected and assessed for cytokine concentration using ELISA, and cell pellets were resuspended in 200 μl of PBS–1% FBS. AM cells obtained from BAL fluid were seeded in 96-well plates and grown overnight. The same amounts of AM cells were treated with serum-free medium for 1 h, and then GFP-PAO1 was used to infect the cells at an MOI of 10:1. After a 1-h incubation at 37°C, the wells were washed and treated with 100 μg/ml polymyxin B for 1 h to kill any remaining extracellular bacteria. The phagocytized bacteria were counted using a Synergy HT fluorometer (BioTek) with 485 (±20)-nm excitation and 528 (±20)-nm emission filters. Background correction was done for autofluorescence.

EMSA. Nuclear extracts from lung tissue samples with different treatments were isolated with a nuclear extraction kit according to the manufacturer's instructions (Pierce, Rockford, IL). Oligonucleotide labeling and binding reactions were performed by using the reagent supplied in the NF-κB p65 electrophoretic mobility shift assay (EMSA) gel shift assay system (Panomics, Inc.). The membrane was exposed using a Bio-Rad imaging system (Bio-Rad, Hercules, CA). The specific mobility shift caused by binding to DNA duplexes was confirmed by adding an excess amount of cold oligonucleotide to the reaction mixture.

Statistical analysis. All statistical analyses were done with SPSS 19.0 software. Data are presented as mean ± standard deviation (SD) and are representative of three experiments. Statistical analysis was performed by Student's *t* test for comparing two groups and by one-way analysis of variance (ANOVA) with Tukey's *post hoc* test for multiple-group comparisons. Differences in the mean values were considered to be significant at a *P* value of <0.05.

RESULTS

Increased infection severity and mortality rates in TRPC1$^{-/-}$ mice. TRPC1 has recently been reported to be activated by LPS to increase cytosolic Ca^{2+} ($[Ca^{2+}]_i$) levels (24); however, this channel protein has not been linked to any infectious disease *per se*. To characterize the physiological relevance of TRPC1 in host defense against bacterial infection *in vivo*, we used TRPC1$^{-/-}$ and WT mice and intranasally instilled a well-characterized strain (PAO1) at 1 × 10^7 CFU into each mouse. As shown in Fig. 1A, TRPC1$^{-/-}$ mice exhibited increased lethality, and at 40 h, all TRPC1$^{-/-}$ mice died, whereas majority of WT mice survived at that time. TRPC1$^{-/-}$ mice exhibited an increased dissemination of *P. aeruginosa* in the area of the thoracic cavity versus WT mice, especially after 12 h of infection. WT mice showed efficient clearance of the invading bacteria from 12 to 24 h after PAO1 infection (Fig. 1B; see Fig. S1A in the supplemental material). At 24 h postinfection, the lungs of TRPC1$^{-/-}$ mice also showed structural damage and increased intensity of bioluminescence compared to those of WT mice (see Fig. S1B in the supplemental material). TRPC1$^{-/-}$ mice also showed significantly increased CFU of PAO1 (approximately 3-fold) in the lung tissue compared to WT mice (Fig. 1C). These findings indicate that TRPC1 may play an important role in host defense.

Leukocyte infiltration in the lung tissue was next assessed. Notably, TRPC1$^{-/-}$ mice showed a decrease in leukocyte count compared to WT mice, while no significant change was observed in controls without PAO1 infection (Fig. 1D and E). Secreted chemokines in the supernatant were detected by ELISA, and reduced production of CCL2 and KC-1 was observed in TRPC1$^{-/-}$ mice (Fig. 1F). These results suggest that low leukocyte infiltrate may be due to the defect in chemokine production in TRPC1$^{-/-}$ mice upon infection. Moreover, decreased infiltration of polymorphonuclear neutrophils (PMN) (a critical phagocyte that eradicates bacteria) in bronchoalveolar lavage (BAL) fluid and serum was observed, which excluded possible effects of the genetic alteration in TRPC1$^{-/-}$ mice (see Fig. S1C in the supplemental material). These data indicate that TRPC1$^{-/-}$ animals also exhibited severely impaired pulmonary inflammatory responses to *P. aeruginosa* challenge.

Bone marrow chimera mouse models confirm the critical role of host defense by TRPC1. To identify the cell types that are critically involved in host defense against bacterial infection *in vivo*, we generated bone marrow chimera mice to investigate whether the effects observed in TRPC1$^{-/-}$ are reversible. Transfer of bone marrow cells from TRPC1$^{-/-}$ to WT mice (after gamma radiation) showed a decrease in survival upon bacterial infection (Fig. 1G), and a corresponding increase in bacterial burdens (see Fig. S2A in the supplemental material) was observed. In contrast, transfer of bone marrow cells from WT to TRPC1$^{-/-}$ mice showed increased survival and decreased bacterial burdens (Fig. 1G; see Fig. S2A in the supplemental material), suggesting that expression of TRPC1 on hematopoietic cells is important for combating PAO1 infection. We next evaluated the functional activity of AM cells obtained from TRPC1$^{-/-}$ mice or WT mice and found that TRPC1$^{-/-}$ AM cells had significantly lowered phagocytosis of GFP-PAO1 than WT AM cells, indicating that TRPC1 may also be involved in the phagocytosis process (see Fig. S2B in the supplemental material). These data recapitulated our observations from TRPC1$^{-/-}$ mice and strongly support our view that TRPC1 plays

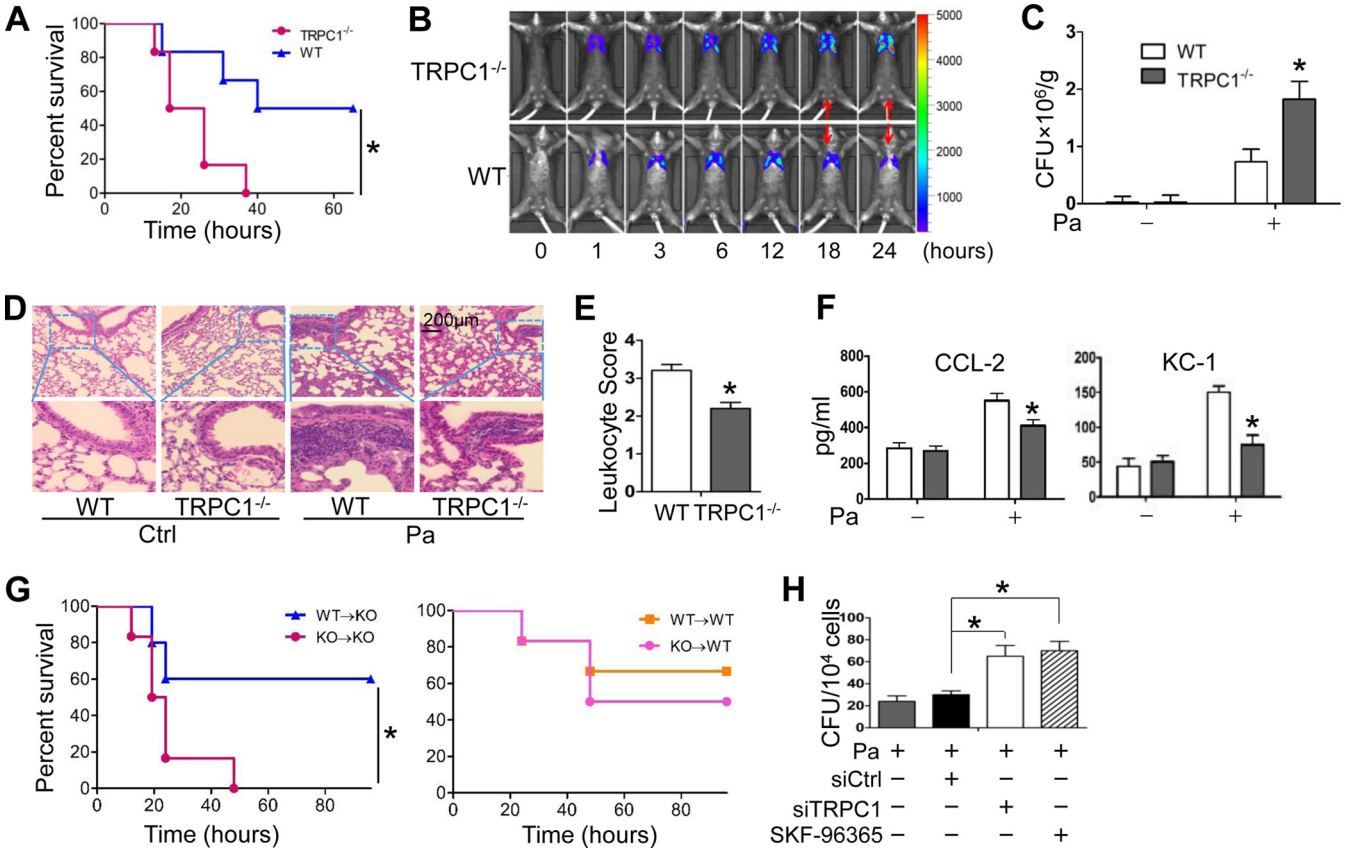

FIG 1 TRPC1$^{-/-}$ mice display increased susceptibility to and mortality rates from *P. aeruginosa* infection. TRPC1$^{-/-}$ mice and WT mice were intranasally infected with 1×10^7 CFU/mouse of PAO1. (A) Survival was determined up to 65 h postinfection and is represented by Kaplan-Meier survival curves ($P = 0.0223$, log rank test; $n = 6$ in each set of animals). (B) *In vivo* imaging of PAO1-infected mice ($n = 5$). TRPC1$^{-/-}$ mice and WT mice were intranasally challenged with 1×10^7 CFU/mouse of Xen-41 (a bioluminescent strain of *P. aeruginosa*). The mice were then monitored up to 24 h. Images showing bioluminescence in the lung at different time points were obtained using the Ivis XRII system. (C to F) The mice from panel A were sacrificed 24 h after *P. aeruginosa* infection, and the lungs were removed. (C) The same quantity of lung tissue was homogenized in PBS and evaluated for bacterial invasion. The data are expressed as CFU/g tissue. (D) Decreased lung inflammation as assessed by morphological analysis. The lungs were embedded in formalin, and sections were analyzed by H&E staining. (E) Leukocyte infiltration scores in lungs from WT and TRPC1$^{-/-}$ mice. (F) BAL fluid was collected, and CCL-2 and KC-1 levels in the supernatant were measured by a standard ELISA. (G) Validation of the function of AM from bone marrow chimera mice. TRPC1$^{-/-}$ and WT mice were irradiated (800 rads) and administered antibiotics via treated drinking water (using 250 units/ml penicillin and 250 μg/ml streptomycin). Ten million bone marrow cells from donor mice were injected into each recipient mouse intravenously immediately after the isolation. Forty-five days later, these mice were challenged with *P. aeruginosa* infection. Survival was determined up to 96 h. (H) MLE-12 cells were transfected with scrambled siRNA or TRPC1 siRNA for 24 h. The cells were then infected with PAO1 at an MOI of 10:1 for 1 h, and polymyxin B (100 μg/ml) was added and left for another 1 h to kill bacteria outside the cells. Cells were treated with 25 μM SKF-96365, a Ca^{2+} channel inhibitor, for 30 min before PAO1 infection. MLE-12 cells were lysed to determine CFU. Survival is represented by Kaplan-Meier survival curves ($P = 0.0489$, log rank test; $n = 5$ or 6 in each set of animals). For other result comparisons, we used one-way ANOVA with a *post hoc* or Student's *t* test. *, $P < 0.05$.

a defense role against *P. aeruginosa* infection. Since bone marrow myeloid cell transfer only partially rescued the resistance to PAO1 infection, it is possible that alveolar type II (ATII) epithelial cells, which are an integral part of the lung innate immunity and a source of proinflammatory cytokines (25, 26), also contribute to host defense, with these two cells together providing almost full resistance to infection. Indeed, TRPC1 siRNA and Ca^{2+} channel inhibitor intervention (SKF-96365) in MLE-12 cells (an alveolar type II epithelial cell line) infected with PAO1 at an MOI of 10:1 showed a significant increase in bacterial loads (Fig. 1H; see Fig. S3A in the supplemental material).

Bacterial infection facilitates Ca^{2+} influx. We thus attempted to evaluate the effect of bacterial infection on $[Ca^{2+}]_i$. Intracellular ER stores were depleted by addition of *P. aeruginosa* LPS, a TLR4 activator, in the absence of extracellular Ca^{2+}. Subsequently, addition of external Ca^{2+}, which initiates Ca^{2+} entry across the plasma membrane to exert cellular functions, resulted in an increase in Ca^{2+} entry in both control and *P. aeruginosa*-treated cells. However, Ca^{2+} entry was significantly increased in bacterium-infected MLE-12 cells, without altering the ER calcium levels (Fig. 2A). Furthermore, depletion of the internal ER store using thapsigargin also showed a similar increase in Ca^{2+} entry in *P. aeruginosa*-treated cells, without affecting basal Ca^{2+} (see Fig. S3C to E in the supplemental material). We also looked at SERCA2 and IP_3R protein levels, but SERCA and IP_3R protein levels were not significantly changed. Similar results were also obtained with cells infected with another human pathogen, the Gram-negative *K. pneumonia*, and an increase in receptor-dependent Ca^{2+} entry was observed upon infection (Fig. 2B). Importantly, the cells transfected with TRPC1 siRNA showed a significantly decreased

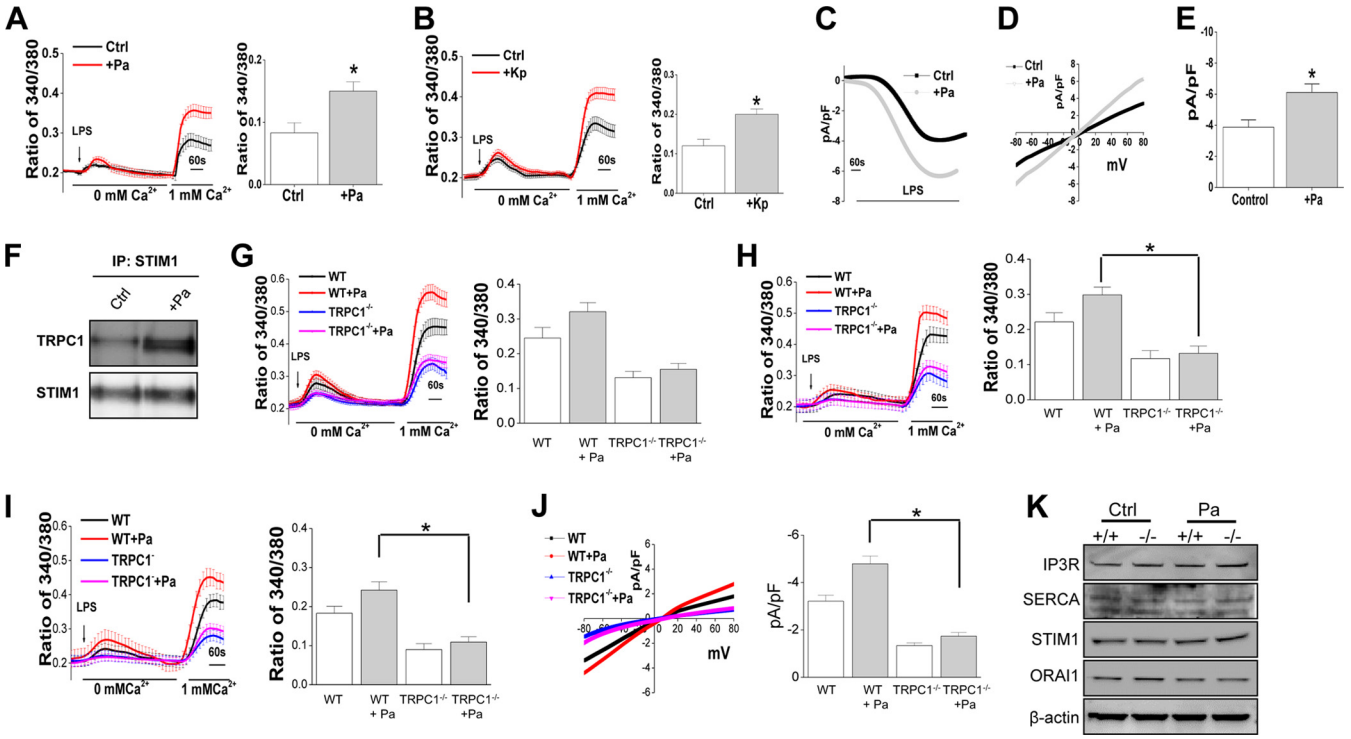

FIG 2 Bacterial infection induces Ca^{2+} influx via the TRPC1 channel. (A and B) Ca^{2+} imaging was performed in the presence of *P. aeruginosa* (Pa) LPS (100 ng/ml) in control, *P. aeruginosa*-treated, or *K. pneumoniae*-treated (15 min) MLE-12 cells. Analog plots of the fluorescence ratio (340/380) from an average of 40 to 60 cells' peak values are shown and were quantified. (C) LPS-induced currents were evaluated in control and *P. aeruginosa*-treated (15 min) MLE-12 cells. The holding potential for current recordings was −80 mV. (D and E) Representative I-V curves under these conditions (D) and the average (8 to 10 recordings) current intensity (at −80 mV) (E) in control and *P. aeruginosa*-treated cells. (F) Coimmunoprecipitates (IP) of MLE-12 cells using STIM1 antibodies in control cells and cells treated with *P. aeruginosa* (30 min) plus LPS (5 min). (G to I) Ca^{2+} imaging was performed in the presence of LPS (100 ng/ml) on primary alveolar epithelial type II cells (G), primary bone marrow-derived macrophages (H), and alveolar macrophages (AM) (I) isolated from wild-type (WT) and $TRPC1^{-/-}$ mice with and without *P. aeruginosa* infection. Analog plots of the fluorescence ratio (340/380) from an average of 40 to 60 cells are shown and were quantified (shown as bar graph). (J) Representative I-V curves for WT and TRPC1 knockdown primary AM upon *P. aeruginosa* infection. (K) Evaluation of IP_3R, SERCA2, STIM1, and ORAI1 protein levels by Western blotting from lung tissues in control and $TRPC1^{-/-}$ mice with and without *P. aeruginosa* treatment. β-Actin served as the loading control. All data (representative of three experiments) are plotted as means ± SD (*, $P < 0.05$), and the statistical methods used were one-way ANOVA coupled with a *post hoc* (three groups or more) or Student *t* (two groups) test unless stated otherwise.

LPS-induced Ca^{2+} entry compared to cells transfected with scrambled siRNA upon infection (see Fig. S4A in the supplemental material). To identify the Ca^{2+} entry channel, electrophysiological recordings were performed, and addition of LPS caused the appearance of an inward current that was nonselective and reversed between 0 and −5 mV (Fig. 2C to E). The channel properties were similar to those previously observed with TRPC1 (8, 11, 16), and PAO1 infection significantly facilitated Ca^{2+} currents without altering the current-voltage (I-V) relationship (Fig. 2D and E), which was inhibited in TRPC1-silenced cells (see Fig. S4B to D in the supplemental material). STIM1 has been shown to be a regulator of TRPC1-mediated Ca^{2+} entry, and upon store depletion, increased STIM1-TRPC1 interaction was observed in *P. aeruginosa*-treated cells (Fig. 2F). Importantly, cells transfected with STIM1 siRNA also showed a significant decrease in LPS-induced Ca^{2+} entry in *P. aeruginosa*-treated cells compared to cells transfected with scrambled siRNA (see Fig. S4E and F in the supplemental material).

To determine the physiological relevance, we isolated primary alveolar epithelial type II (ATII) cells, bone marrow-derived cells, and primary alveolar macrophages (AM) isolated from control (WT) and $TRPC1^{-/-}$ mice to investigate whether TRPC1 contributes to the Ca^{2+}-mediated cell signals in these cells in response to bacterial infection. Interestingly, the results showed that Ca^{2+} influx was significantly increased in all three types of cells isolated from WT mice (albeit with ATII cells being the strongest) that were infected with *P. aeruginosa*, compared to uninfected controls (Fig. 2G to J). However, no significant increase in Ca^{2+} influx was observed in *P. aeruginosa*-infected cells isolated from $TRPC1^{-/-}$ mice (Fig. 2G to I). In addition, Ca^{2+} influx *per se* was significantly decreased in $TRPC1^{-/-}$ cells (Fig. 2G to I). Furthermore, the channel properties (I-V curve) in AM cells (Fig. 2J) were similar to those shown in Fig. 2D, which were again significantly decreased in $TRPC1^{-/-}$ cells. Importantly, protein levels of IP_3R, SERCA2, STIM1, and Orai1 were not significantly changed in $TRPC1^{-/-}$ mice treated with *P. aeruginosa* (Fig. 2K), indicating that the loss of *P. aeruginosa*-induced Ca^{2+} entry was primarily due to the loss of TRPC1. This phenomenon was further validated in alveolar macrophages isolated from bone marrow chimera mice (see Fig. S2C and D in the supplemental material). Pretreatment of PAO1 also facilitated Ca^{2+} influx induced by 1-oleoyl-2-acetyl-glycerol (OAG); however, prolonged treatment with OAG was needed for a significant increase in $[Ca^{2+}]_i$, and the relative Ca^{2+} influx was significantly lower than with LPS (see Fig. S4G in the supplemen-

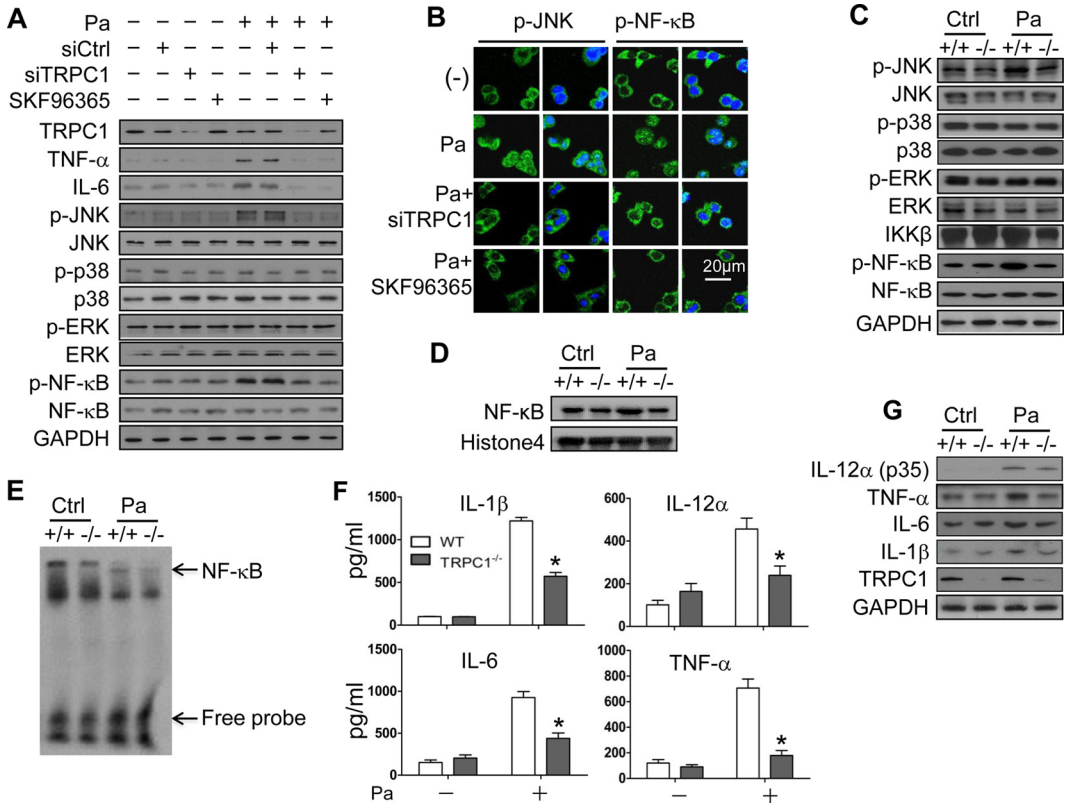

FIG 3 TRPC1 silencing suppresses the JNK/NF-κB pathway by *P. aeruginosa* infection. (A) MLE-12 cells were transfected with scrambled siRNA or TRPC1 siRNA for 24 h. The cells were then infected with PAO1 at an MOI of 10:1 for 1 h, and polymyxin B (100 μg/ml) was added and left for another 1 h to kill bacteria outside the cells. Cells were treated with 25 μM SKF-96365 for 30 min before PAO1 infection. The samples were used to determine activation of the JNK/NF-κB pathways and other related signaling proteins by Western blotting. (B) Confocal fluorescence results showed the translocation of p-JNK and p-NF-κB p65 (Ser536) in MLE-12 cells from panel A using immune staining. DAPI was used to stain the nucleus. (C) WT and TRPC1$^{-/-}$ mice were intranasally infected with 1×10^7 CFU of PAO1 for 24 h ($n = 5$). p-JNK, JNK, p-p38, p38, p-ERK, ERK, IKKβ, and p-NF-κB p65 (Ser536) levels were determined by Western blotting from lung tissues. GAPDH served as the loading control. (D) The nuclear fraction of lung tissue of mice infected with PAO1 for 24 h was isolated using a nuclear extraction kit (Pierce; number 78833). NF-κB expression was detected by Western blotting, and histone 4 was used as a loading control. (E) EMSA was performed using a biotin-labeled probe, which contains only a single copy of the 21-bp element. Shown are results from reactions performed in the presence of WT mouse lung tissue nuclear extract (2 μg; lane 1), TRPC1 KO mouse lung tissue nuclear extract (2 μg; lane 2), *P. aeruginosa*-treated WT mouse lung tissue nuclear extract (2 μg; lane 3), and *P. aeruginosa*-treated TRPC1 KO mouse lung tissue nuclear extract (2 μg; lane 4) (24-h *P. aeruginosa* infection). (F) Cytokines in the BAL fluid from panel C were measured using ELISA. (G) Lung tissues from panel C were lysed to assess the levels of various cytokines. One-way ANOVA with a *post hoc* or Student *t* test was used. *, $P < 0.05$. The data are representative of three experiments.

tal material). Overall, these results indicate that both *P. aeruginosa* and *K. pneumoniae* infections facilitate $[Ca^{2+}]_i$ via the TRPC1 channel.

TRPC1 deficiency hampers the JNK/NF-κB pathway against *P. aeruginosa* infection. To evaluate the downstream signaling events, we evaluated several kinase proteins and cytokines in cell culture models. Both TRPC1 siRNA-transfected cells and Ca^{2+} entry inhibitor (SKF-96365)-treated cells demonstrated a decrease in the phosphorylation of JNK and NF-κB, which may be associated with the lowered secretion of IL-6 and TNF-α, whereas there was no significant change in the phosphorylation of p38 and ERK1/2 (Fig. 3A; see Fig. S5A in the supplemental material). These data indicate that the infection phenotypes may be attributed to a dysregulated proinflammatory response through the TRPC1/JNK/NF-κB axis. Further, immunofluorescence showed that both JNK and NF-κB were activated and were translocated into the nucleus in control MLE-12 cells but not in TRPC1 siRNA-transfected or SKF-96365-treated MLE-12 cells (Fig. 3B), suggesting that TRPC1 may facilitate the nuclear translocation of these transcription factors to initiate inflammatory cytokine mRNA synthesis when the host is challenged with bacteria.

To further validate the inflammatory response in MLE-12 cells, we assessed the expression and activation levels of these proteins *in vivo*. Importantly, the phosphorylation level of JNK was found to be decreased in the lungs of TRPC1$^{-/-}$ mice compared to those of WT mice (Fig. 3C; see Fig. S5B in the supplemental material). Our data also showed that IKKβ expression and NF-κB phosphorylation significantly decreased in the lungs of TRPC1$^{-/-}$ mice compared to those of WT mice (Fig. 3C; see Fig. S5B in the supplemental material). Additionally, JNK and NF-κB were activated in a time-dependent manner upon bacterial infection (see Fig. S6 in the supplemental material).

To convincingly demonstrate the activation of NF-κB, we also examined the translocation of p-JNK and p-NF-κB using pharmaceutical inhibitors. The nuclear translocation of NF-κB (p65 subunit) was abolished by both the JNK inhibitor and the NF-κB inhibitor as demonstrated by immunofluorescence staining. However, JNK was still activated and translocated into the nucleus

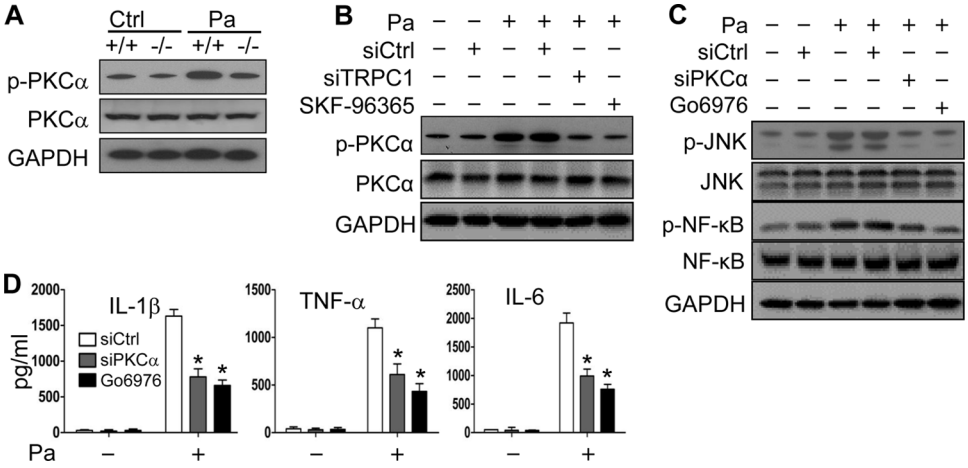

FIG 4 PKCα as the TRPC1 effector mediates JNK/NF-κB activation and inflammatory responses. (A) Mice were intranasally infected with 1×10^7 CFU of PAO1 for 24 h ($n = 5$). Lung tissues were lysed to assess the levels of p-PKCα and PKCα by Western blotting. GAPDH served as the loading control. (B) MLE-12 cells were transfected with various siRNAs (50 nM). After 24 h, the cells were infected with PAO1 at an MOI of 10:1 for 1 h. Cells were treated with 25 μM SKF-96365 for 30 min before PAO1 infection. Cells were lysed and were used to assess the levels of p-PKCα and PKCα. (C) MLE-12 cells were transfected with scrambled or PKCα siRNA (50 nM) for 24 h. The cells were then infected with PAO1 at an MOI of 10:1 for 1 h. The cells were treated with 3 μM PKCα inhibitor (Go6976) 30 min before PAO1 infection. Equal numbers of the cells were lysed and were used to assess the levels of p-JNK and p-NF-κB p65 (Ser536). GAPDH served as the loading control. (D) MH-S cells were transfected with various siRNAs (50 nM) for 24 h and then infected with PAO1 at an MOI of 10:1 for 1 h, and polymyxin B (100 μg/ml) was added into the medium and left for another 15 h. Cells were treated with 3 μM PKCα inhibitor (Go6976) 30 min before bacterial infection. Different cytokines in the supernatant were measured by a standard ELISA.

in the presence of the NF-κB inhibitor (see Fig. S7A in the supplemental material). Consistent with the immunofluorescence analysis, a luciferase promoter assay showed the activation of NF-κB in the control group, but this was significantly impaired in the presence of either the JNK inhibitor (SP600125) or the Ca^{2+} entry inhibitor (SKF-96365) (see Fig. S7B in the supplemental material). Moreover, nuclear fractions of lung tissue were also isolated to evaluate NF-κB levels by Western blotting. As shown in Fig. 3D, NF-κB levels increased in the nuclei of WT mice upon *P. aeruginosa* infection, while they were not significantly changed in *P. aeruginosa*-infected TRPC1$^{-/-}$ mice versus control mice. To clearly identify molecular evidence of the nuclear translocation, we performed an electrophoretic mobility shift assay (EMSA) and showed obviously retarded mobility in WT mice versus TRPC1$^{-/-}$ mice (Fig. 3E). Although lung homogenates contain a myriad of cells, alveolar epithelial cells are the main cell population and thus likely contribute predominantly to the result of NF-κB translocation.

To further investigate whether TRPC1 directly impacts cytokine production *in vivo*, we measured cytokines in BAL fluid and noted a significant difference in inflammatory cytokines between TRPC1$^{-/-}$ mice and control mice. In the lungs of PAO1-infected TRPC1$^{-/-}$ mice, the cytokine levels of IL-1β, IL-12α (p35), IL-6, and TNF-α were significantly decreased compared to those in WT mice (Fig. 3F). These results were further corroborated with Western blotting, with decreased levels of IL-1β, IL-12α (p35), IL-6, and TNF-α in TRPC1$^{-/-}$ lung tissues infected with PAO1 (Fig. 3G; see Fig. S5C in the supplemental material). Overall, these findings indicate that TRPC1$^{-/-}$ mice exhibit impaired proinflammatory responses following PAO1 infection compared to WT mice.

PKCα is a critical link for TRPC1-mediated JNK/NF-κB signaling activation and inflammatory responses. Protein kinase Cα (PKCα) has been shown to be upstream in the regulation of JNK and NF-κB signaling (27, 28). We thus investigated whether PKCα is the crucial link for TRPC1-meidated JNK and NF-κB activation and inflammatory response. As shown in Fig. 4A and in Fig. S8A in the supplemental material, deletion of TRPC1 markedly reduced the phosphorylated PKCα (Thr638) level induced by bacterial infection. Similar to the case for TRPC1$^{-/-}$ mice, TRPC1-silenced MLE-12 cells also failed to elicit the activation of PKCα (Fig. 4B; see Fig. S8B in the supplemental material). Collectively, these data indicate that PKCα phosphorylation was increased following bacterial infection in WT mouse lungs and MLE-12 cells but decreased in both TRPC1$^{-/-}$ mouse lungs and TRPC1-silenced MLE-12 cells. Thus, TRPC1 may be a previously undiscovered player between bacterial infection and PKCα activation.

Using pharmacological inhibitors and genetic silencing strategies, we showed that cells treated with PKCα inhibitor or transfected with PKCα siRNA exhibited decreased phosphorylation of JNK and NF-κB (Fig. 4C; see Fig. S3B and S8C in the supplemental material) upon bacterial infection. Moreover, PKCα or TRPC1 silencing or PKC inhibitor treatment also reduced the expression of IL-1β, IL-6, and TNF-α compared to that in controls (Fig. 4D). Taken together, these data indicate that TRPC1 activated the JNK/NF-κB signaling pathway by directly regulating PKCα, leading to proinflammatory cytokine release.

To determine whether TRPC1/PKCα signaling has a general role in inflammatory responses to other bacterial infections, we also used *K. pneumoniae* and another *P. aeruginosa* strain (PAK, a more cytotoxic strain than PAO1) to infect MH-S cells to test the corresponding immunity. Similar to the results of PAO1 infection, the expression levels of IL-1β, IL-6, and TNF-α were lower in MH-S cells transfected with TRPC1 siRNA or PKCα siRNA than in cells transfected with siRNA negative controls (see Fig. S9 in the supplemental material), suggesting that TRPC1/PKCα signaling has a ubiquitous activity in regulating inflammatory responses in both alveolar macrophages and epithelial cells.

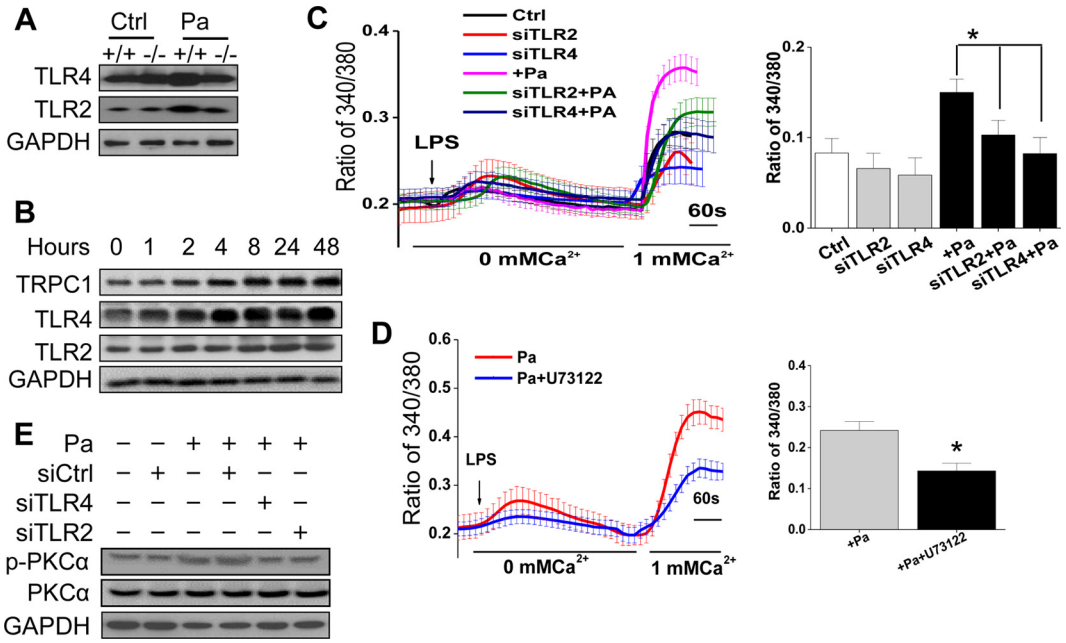

FIG 5 TLR4 is essential for TRPC1 function upon *P. aeruginosa* infection. (A) WT and TRPC1$^{-/-}$ mice were intranasally infected with 1×10^7 CFU of PAO1 for 24 h ($n = 5$). Lung tissues were lysed to assess the levels of various proteins using different antibodies as indicated. GAPDH served as the loading control. (B) Time-dependent expression of TRPC1 and TLR2/4 in the lung tissues of WT mice. The mice were infected with PAO1 for up to 48 h. (C) Ca^{2+} imaging was performed in the presence of LPS under various conditions in MLE-12 cells. Analog plots and quantification of the fluorescence ratio (340/380) from an average of 50 to 80 cells are shown. (D) Ca^{2+} imaging was performed in the presence of LPS under treatment with PLC-γ inhibitor (U73122) in MH-S cells infected with PAO1. Analog plots of the fluorescence ratio (340/380) from an average of 50 to 80 cells are shown. Quantification of the fluorescence ratio (340/380) from an average of 100 to 125 cells infected with PAO1 under various conditions is shown. (E) MLE-12 cells were transfected with various siRNAs (50 nM). After 24 h, the cells were infected with PAO1 at an MOI of 10:1 for 1 h. Cells were lysed and were used to assess the levels of p-PKCα and PKCα. One-way ANOVA with a *post hoc* test was used. *, $P < 0.05$. The data are representative of three experiments.

TLR4 is essential for TRPC1 function upon *P. aeruginosa* infection. Since the production of DAG and IP_3-mediated Ca^{2+} entry from the plasma membrane can be induced by TLR4 after the treatment of lipoproteins, lipoteichoic acid, or LPS, which facilitates the translocation of PKCα from the cytosol to the plasma membrane (29, 30), we reasoned that TLRs may activate the TRPC1 channel to regulate PKCα signaling. Importantly, following PAO1 infection, TRPC1$^{-/-}$ mice showed decreased TLR expression compared to WT mice (Fig. 5A; see Fig. S10A in the supplemental material). Additionally, expression levels of TRPC1 and TLR2/4 proteins were increased in a time-dependent manner upon bacterial infection, with TLR4 increasing earlier and more strongly than TLR2 (Fig. 5B; see Fig. S10B in the supplemental material). Moreover, silencing of TLRs by use of siRNAs, as validated in our previous report (31), had no effects on ER Ca^{2+} levels, but the bacterium-dependent increase in Ca^{2+} entry (as observed in Fig. 2) was significantly inhibited (Fig. 5C; see Fig. S11A in the supplemental material). Coupled with LPS-mediated TRPC1 channel excitation, these data indicate that time-dependent TLR4 signaling may contribute to TRPC1-mediated Ca^{2+} entry and to its associated downstream events, including cytokine secretion.

To further establish the link between TLR4 and TRPC1, we investigated whether store depletion is needed for TRPC1 activation. Since PLC-γ has been implicated in LPS-induced TLR4-mediated Ca^{2+} release from the ER stores, which is necessary for regulating cellular functions of TRPC1 (32–34), we then investigated the effect of PLC-γ on Ca^{2+} mobilization in our model. As expected, inhibition of PLC-γ by U73122 significantly decreased LPS-induced Ca^{2+} entry and TRPC1 expression in a time-dependent manner (Fig. 5D). Similarly, inhibition of TLR4 using the chemical antagonist E5564 (kindly provided by Eisai Co.) also showed a decrease in TRPC1-mediated Ca^{2+} currents (see Fig. S11B in the supplemental material). Importantly, these Ca^{2+} currents were initiated by store depletion, as IP_3 in the patch pipette showed similar Ca^{2+} currents, which were not further potentiated by the addition of LPS and were also not inhibited by TLR4 inhibition (see Fig. S11C in the supplemental material), suggesting that in bacterial infection, TRPC1 activation is involved in PLC-γ signaling in the TLR4-dependent store depletion mechanism.

We next assessed the role of TLR2/4 in PKCα signaling and showed that PKCα phosphorylation was decreased when cells were transfected with either TLR2 siRNA or TLR4 siRNA (Fig. 5E; see Fig. S10C in the supplemental material), while TLR4 played a dominant role. These findings suggest that TLR4 is essential to link TRPC1 to PKCα in bacterial infection.

Thus, the overall data demonstrate that the TRPC1-PKCα-JNK-NF-κB circuit is critically involved in Gram-negative bacterial infection, which modulates the proinflammatory response against the invading bacteria. A breakdown in this defense mechanism results in a significantly weakened host defense, leading to a severe infection phenotype as observed in TRPC1$^{-/-}$ mice and cultured cells. To illustrate the molecular mechanism involved in bacterial infection, we illustrated a model for the cellular signaling, which shows that Gram-negative bacterial infection induces TLR4 activation leading to store depletion followed by the activa-

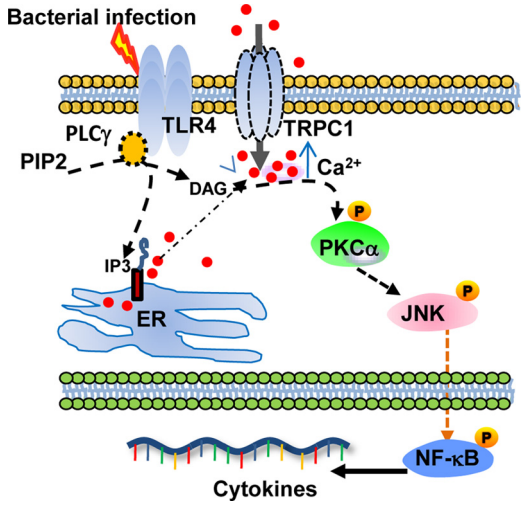

FIG 6 Schematic describing the proposed TRPC1/PKCα/JNK/NF-κB axis involved in the dysregulated proinflammatory response during bacterial infection.

tion of TRPC1, which subsequently mediates inflammatory response through the TRPC1/PKCα/JNK/NF-κB pathway (Fig. 6).

DISCUSSION

Previous studies have demonstrated that TRPC1 is associated with lipid rafts, a critical cell signaling initiator formed during bacterial infections; we thus surmise that TRPC1 may play a key role in the host response against bacterial infection in lung epithelial cells (35). Although studies have illustrated the role of TRPC1 in the cell cycle, cell proliferation, and many other processes (6, 11, 36), its role in innate immunity against whole microorganisms is not yet identified. In this study, we showed that *P. aeruginosa* infection facilitated the activation of Ca^{2+} influx via the TRPC1 channel. Furthermore, the endogenous Ca^{2+} entry channel that was activated by TLR was similarly observed as TRPC1-dependent I_{Soc} currents (16), which were increased in *P. aeruginosa*- and *K. pneumoniae*-infected cells. Our findings suggest that TRPC1 may augment immunity against Gram-negative bacterial infection.

Combating bacterial infection requires robust inflammatory responses, but excessive inflammation can dampen immunity and thus worsen disease. Our current study indicates that TRPC1$^{-/-}$ mice succumb to infection due to decreased inflammatory responses and subsequent ineffective bacterial clearance. It has been suggested that TPRC1 is necessary for lymphocyte biological function and is a regulator of lung hyperresponsiveness during the allergen-induced pulmonary response (37). Previous findings also indicate that lung epithelial cells may play a key role in the production of proinflammatory cytokines (25, 26). Consistent with previous studies, we also found that activation of two signaling proteins (JNK and NF-κB) was blunted in both TPRC1-silenced epithelial cells and TRPC1$^{-/-}$ mice (38, 39). Critically, we reveal a new mechanism by identifying that Ca^{2+} entry via TRPC1 is essential for the activation. As expected, JNK inhibition decreased NF-κB activation and reduced inflammatory responses, indicating that JNK activation is required for NF-κB activation and initiation of the downstream inflammatory response. Interestingly, others reported that p38 was involved in the NF-κB pathway, and this variation may be related to the model system used; perhaps *in vivo* signaling is involved a complex and coordinated regulatory mechanism (40, 41). Taken together, our data suggest that TRPC1 initiates a positive regulation in the JNK/NF-κB pathway, which seems important for control of human pathogens. Therefore, TRPC1 deficiency leads to a lowered cytokine response and thereby a worsened host defense phenotype.

To further probe how TRPC1 can regulate the activation of JNK and NF-κB, we focused on the role of PKCα, a serine- and threonine-specific protein kinase that can regulate the activation of JNK and NF-κB (27, 28). Activation of PKCα is induced by Ca^{2+} and the second messenger DAG (42, 43); however, the ion channel that initiates Ca^{2+} entry, thereby regulating PKC activity, is not yet identified. Here, we show that TRPC1 regulates the activation of PKCα, which was dependent on TRPC1-mediated Ca^{2+} entry.

In addition, TLR4 is also a critical signal that induces the production of second messengers while serving as a pathogen recognition receptor (29, 30, 44) to activate the TRPC1 channel. Importantly, we identified that TRPC1-mediated activation of PKCα can induce the activation of JNK and NF-κB. These observations offered a model describing that bacterial infection induces TLR4-mediated activation of TRPC1, which initiates Ca^{2+} entry to activate PKCα, which functions as an effector in inducing JNK and NF-κB, which are critical for cytokine production and bacterial clearance. We noticed that TLR4 responds to *P. aeruginosa* infection earlier and more strongly than TLR2, that the TRPC1 channel is also excited by LPS, and that the signaling is impaired by both TLR4 siRNA silencing and the E5564 inhibitor. These data indicate that TLR4 is upstream of the TRPC1 pathway, though TLR2's involvement cannot be completely excluded at this time. In addition, the function of PLC-γ in Ca^{2+} mobilization in our system was consistent with that described in previous reports (32–34). These data indicate that the PLC-γ pathway plays an important role in bacterial ligand-induced TRPC1 activation. However, the detailed mechanism of PLC-γ in the activation of TRPC1 and whether other signals also contribute to this process need further investigation. Moreover, PKCα has been shown to phosphorylate TRPC1 and serves as an important determinant of Ca^{2+} entry, indicating that there might also be positive feedback in TRPC1/PKCα-mediated immune signaling (45). In a more recent study, TRPC1 KO mice exhibited decreased IL-1β levels in *Escherichia coli* LPS-mediated sepsis models, and this variation again may be due to different LPS species involved (15). Nevertheless, the data from the current study are largely based on a bacterial model, which has not been evaluated before. Our study also evaluated other calcium channels and their regulators (i.e., STIM1) for protein expression and function, as well as ER-mediated calcium entry. Although TRPC1 may function as an immunity regulator in bacterial infection via STIM1 signals, there was no significant alteration in protein expression for STIM1/Orai1, IPR3, and SERCA1 (Fig. 2K), suggesting that TRPC1 appears to be a dominant player during bacterial infection, particularly in its associated inflammatory responses. Although TRPC1 is identified as a new immunity regulator, host immunity may be related to an increasingly complex network, and other Ca^{2+} entry channels (i.e., STIM1/Orai1) might also play a role in this process.

Overall, our data demonstrate a typical phenotype of bacterial infection in TRPC1$^{-/-}$ mice and suggest an important role for TRPC1 in the innate immunity against human pathogens. TRPC1 deficiency impaired the phagocytic ability and other immune de-

fense mechanisms, resulting in decreased infiltration of leukocytes into the lung and a greatly attenuated inflammatory response. In particular, the impaired immune function in TRPC1$^{-/-}$ mice is highly attributable to dysregulatory effects on the TRPC1/PKCα/JNK/NF-κB axis, which governs the inflammatory process. Furthermore, at the upstream point of this immune circuit, TLR4-mediated activation of TRPC1 followed by PKCα is required to initiate and control the host defense response. Collectively, these findings provide novel insight into the role of TRPC1 in the innate immune reaction against bacteria, indicating novel targets to combat bacterial invasion.

ACKNOWLEDGMENTS

We acknowledge the use of the Edward C. Carlson Imaging and Image Analysis Core Facility and appreciate the gift of TLR4 antagonist E5564, kindly provided by Eisai Co.

This project was supported by FAMRI (no. 103007) and grants NIH P20 RR017699, NIH R01 AI109317-01A1, and AI101973-01 to M.W., grants AI097532-01A1 and R01 DE017102 to B.B.S., National Natural Science Foundation of China (no. 81202324) and China Postdoctoral Science Foundation (no. 2014T70873) grants to X.Z., and an Intramural Research Program of the NIH (project Z01-ES101864) grant to L.B.

We declare that we have no conflict of interest.

X.Z., Y.Y., Y.S., X.L., B.P., W.W., S.T., C.H., and M.W. performed experiments. L.B. contributed reagents and edited the paper. Z.Z. contributed resources. X.Z., Y.-Q.W., B.B.S., and M.W conceived and designed the studies and wrote the paper.

REFERENCES

1. **Sun HY, Fujitani S, Quintiliani R, Yu VL.** 2011. Pneumonia due to Pseudomonas aeruginosa. II. Antimicrobial resistance, pharmacodynamic concepts, and antibiotic therapy. Chest **139:**1172–1185.
2. **Cortes G, Alvarez D, Saus C, Alberti S.** 2002. Role of lung epithelial cells in defense against Klebsiella pneumoniae pneumonia. Infect Immun **70:**1075–1080. http://dx.doi.org/10.1128/IAI.70.3.1075-1080.2002.
3. **Yuan K, Huang C, Fox J, Gaid M, Weaver A, Li G, Singh BB, Gao H, Wu M.** 2011. Elevated inflammatory response in caveolin-1-deficient mice with Pseudomonas aeruginosa infection is mediated by STAT3 protein and nuclear factor kappaB (NF-kappaB). J Biol Chem **286:**21814–21825. http://dx.doi.org/10.1074/jbc.M111.237628.
4. **Guo Q, Shen N, Yuan K, Li J, Wu H, Zeng Y, JFox 3rd, Bansal AK, Singh BB, Gao H, Wu M.** 2012. Caveolin-1 plays a critical role in host immunity against Klebsiella pneumoniae by regulating STAT5 and Akt activity. Eur J Immunol **42:**1500–1511. http://dx.doi.org/10.1002/eji.201142051.
5. **Lavoie EG, Wangdi T, Kazmierczak BI.** 2011. Innate immune responses to Pseudomonas aeruginosa infection. Microbes Infect **13:**1133–1145. http://dx.doi.org/10.1016/j.micinf.2011.07.011.
6. **Pani B, Bollimuntha S, Singh BB.** 2012. The TR (i)P to Ca(2)(+) signaling just got STIMy: an update on STIM1 activated TRPC channels. Front Biosci **17:**805–823. http://dx.doi.org/10.2741/3958.
7. **Yuan JP, Zeng W, Huang GN, Worley PF, Muallem S.** 2007. STIM1 heteromultimerizes TRPC channels to determine their function as store-operated channels. Nat Cell Biol **9:**636–645. http://dx.doi.org/10.1038/ncb1590.
8. **Zeng W, Yuan JP, Kim MS, Choi YJ, Huang GN, Worley PF, Muallem S.** 2008. STIM1 gates TRPC channels, but not Orai1, by electrostatic interaction. Mol Cell **32:**439–448. http://dx.doi.org/10.1016/j.molcel.2008.09.020.
9. **Madsen CP, Klausen TK, Fabian A, Hansen BJ, Pedersen SF, Hoffmann EK.** 2012. On the role of TRPC1 in control of Ca2+ influx, cell volume, and cell cycle. Am J Physiol Cell Physiol **303:**C625–C634. http://dx.doi.org/10.1152/ajpcell.00287.2011.
10. **Kuang CY, Yu Y, Wang K, Qian DH, Den MY, Huang L.** 2012. Knockdown of transient receptor potential canonical-1 reduces the proliferation and migration of endothelial progenitor cells. Stem Cells Dev **21:**487–496. http://dx.doi.org/10.1089/scd.2011.0027.
11. **Selvaraj S, Sun Y, Singh BB.** 2010. TRPC channels and their implication in neurological diseases. CNS Neurol Disord Drug Targets **9:**94–104. http://dx.doi.org/10.2174/187152710790966650.
12. **Ong HL, Cheng KT, Liu X, Bandyopadhyay BC, Paria BC, Soboloff J, Pani B, Gwack Y, Srikanth S, Singh BB, Gill DL, Ambudkar IS.** 2007. Dynamic assembly of TRPC1-STIM1-Orai1 ternary complex is involved in store-operated calcium influx. Evidence for similarities in store-operated and calcium release-activated calcium channel components. J Biol Chem **282:**9105–9116.
13. **Zhang H, Clemens RA, Liu F, Hu Y, Baba Y, Theodore P, Kurosaki T, Lowell CA.** 2014. STIM1 calcium sensor is required for activation of the phagocyte oxidase during inflammation and host defense. Blood **123:**2238–2249. http://dx.doi.org/10.1182/blood-2012-08-450403.
14. **Gandhirajan RK, Meng S, Chandramoorthy HC, Mallilankaraman K, Mancarella S, Gao H, Razmpour R, Yang XF, Houser SR, Chen J, Koch WJ, Wang H, Soboloff J, Gill DL, Madesh M.** 2013. Blockade of NOX2 and STIM1 signaling limits lipopolysaccharide-induced vascular inflammation. J Clin Invest **123:**887–902. http://dx.doi.org/10.1172/JCI65647.
15. **Py BF, Jin M, Desai BN, Penumaka A, Zhu H, Kober M, Dietrich A, Lipinski MM, Henry T, Clapham DE, Yuan J.** 2014. Caspase-11 controls interleukin-1beta release through degradation of TRPC1. Cell Rep **6:**1122–1128. http://dx.doi.org/10.1016/j.celrep.2014.02.015.
16. **Liu X, Cheng KT, Bandyopadhyay BC, Pani B, Dietrich A, Paria BC, Swaim WD, Beech D, Yildrim E, Singh BB, Birnbaumer L, Ambudkar IS.** 2007. Attenuation of store-operated Ca2+ current impairs salivary gland fluid secretion in TRPC1(−/−) mice. Proc Natl Acad Sci U S A **104:**17542–17547. http://dx.doi.org/10.1073/pnas.0701254104.
17. **Kulasakara H, Lee V, Brencic A, Liberati N, Urbach J, Miyata S, Lee DG, Neely AN, Hyodo M, Hayakawa Y, Ausubel FM, Lory S.** 2006. Analysis of Pseudomonas aeruginosa diguanylate cyclases and phosphodiesterases reveals a role for bis-(3′-5′)-cyclic-GMP in virulence. Proc Natl Acad Sci U S A **103:**2839–2844. http://dx.doi.org/10.1073/pnas.0511090103.
18. **Lawlor MS, Hsu J, Rick PD, Miller VL.** 2005. Identification of Klebsiella pneumoniae virulence determinants using an intranasal infection model. Mol Microbiol **58:**1054–1073. http://dx.doi.org/10.1111/j.1365-2958.2005.04918.x.
19. **Priebe GP, Brinig MM, Hatano K, Grout M, Coleman FT, Pier GB, Goldberg JB.** 2002. Construction and characterization of a live, attenuated aroA deletion mutant of Pseudomonas aeruginosa as a candidate intranasal vaccine. Infect Immun **70:**1507–1517. http://dx.doi.org/10.1128/IAI.70.3.1507-1517.2002.
20. **Sun Y, Selvaraj S, Varma A, Derry S, Sahmoun AE, Singh BB.** 2013. Increase in serum Ca2+/Mg2+ ratio promotes proliferation of prostate cancer cells by activating TRPM7 channels. J Biol Chem **288:**255–263. http://dx.doi.org/10.1074/jbc.M112.393918.
21. **Selvaraj S, Sun Y, Watt JA, Wang S, Lei S, Birnbaumer L, Singh BB.** 2012. Neurotoxin-induced ER stress in mouse dopaminergic neurons involves downregulation of TRPC1 and inhibition of AKT/mTOR signaling. J Clin Invest **122:**1354–1367. http://dx.doi.org/10.1172/JCI61332.
22. **Wu M, Stockley PG, Martin WJ, II.** 2002. An improved Western blotting technique effectively reduces background. Electrophoresis **23:**2373–2376. http://dx.doi.org/10.1002/1522-2683(200208)23:15<2373::AID-ELPS2373>3.0.CO;2-W.
23. **Klesney-Tait J, Keck K, Li X, Gilfillan S, Otero K, Baruah S, Meyerholz DK, Varga SM, Knudson CJ, Moninger TO, Moreland J, Zabner J, Colonna M.** 2013. Transepithelial migration of neutrophils into the lung requires TREM-1. J Clin Invest **123:**138–149. http://dx.doi.org/10.1172/JCI64181.
24. **Buyck JM, Verriere V, Benmahdi R, Higgins G, Guery B, Matran R, Harvey BJ, Faure K, Urbach V.** 2013. P. aeruginosa LPS stimulates calcium signaling and chloride secretion via CFTR in human bronchial epithelial cells. J Cyst Fibros **12:**60–67. http://dx.doi.org/10.1016/j.jcf.2012.06.007.
25. **Kannan S, Huang H, Seeger D, Audet A, Chen Y, Huang C, Gao H, Li S, Wu M.** 2009. Alveolar epithelial type II cells activate alveolar macrophages and mitigate P. aeruginosa infection. PLoS One **4:**e4891. http://dx.doi.org/10.1371/journal.pone.0004891.
26. **Amano H, Morimoto K, Senba M, Wang H, Ishida Y, Kumatori A, Yoshimine H, Oishi K, Mukaida N, Nagatake T.** 2004. Essential contribution of monocyte chemoattractant protein-1/C-C chemokine ligand-2 to resolution and repair processes in acute bacterial pneumonia. J Immunol **172:**398–409. http://dx.doi.org/10.4049/jimmunol.172.1.398.
27. **Lopez-Bergami P, Habelhah H, Bhoumik A, Zhang W, Wang LH, Ronai Z.** 2005. RACK1 mediates activation of JNK by protein kinase C. Mol Cell **19:**309–320. http://dx.doi.org/10.1016/j.molcel.2005.06.025.
28. **Trushin SA, Pennington KN, Carmona EM, Asin S, Savoy DN, Billadeau DD, Paya CV.** 2003. Protein kinase Calpha (PKCalpha) acts

upstream of PKCtheta to activate IkappaB kinase and NF-kappaB in T lymphocytes. Mol Cell Biol **23:**7068–7081. http://dx.doi.org/10.1128/MCB.23.19.7068-7081.2003.

29. **Tauseef M, Knezevic N, Chava KR, Smith M, Sukriti S, Gianaris N, Obukhov AG, Vogel SM, Schraufnagel DE, Dietrich A, Birnbaumer L, Malik AB, Mehta D.** 2012. TLR4 activation of TRPC6-dependent calcium signaling mediates endotoxin-induced lung vascular permeability and inflammation. J Exp Med **209:**1953–1968. http://dx.doi.org/10.1084/jem.20111355.
30. **Machata S, Tchatalbachev S, Mohamed W, Jansch L, Hain T, Chakraborty T.** 2008. Lipoproteins of Listeria monocytogenes are critical for virulence and TLR2-mediated immune activation. J Immunol **181:**2028–2035. http://dx.doi.org/10.4049/jimmunol.181.3.2028.
31. **Zhou X, Li X, Ye Y, Zhao K, Zhuang Y, Li Y, Wei Y, Wu M.** 2014. MicroRNA-302b augments host defense to bacteria by regulating inflammatory responses via feedback to TLR/IRAK4 circuits. Nat Commun **5:**3619. http://dx.doi.org/10.1038/ncomms4619.
32. **Aki D, Minoda Y, Yoshida H, Watanabe S, Yoshida R, Takaesu G, Chinen T, Inaba T, Hikida M, Kurosaki T, Saeki K, Yoshimura A.** 2008. Peptidoglycan and lipopolysaccharide activate PLCgamma2, leading to enhanced cytokine production in macrophages and dendritic cells. Genes Cells **13:**199–208. http://dx.doi.org/10.1111/j.1365-2443.2007.01159.x.
33. **Chiang CY, Veckman V, Limmer K, David M.** 2012. Phospholipase Cgamma-2 and intracellular calcium are required for lipopolysaccharide-induced Toll-like receptor 4 (TLR4) endocytosis and interferon regulatory factor 3 (IRF3) activation. J Biol Chem **287:**3704–3709. http://dx.doi.org/10.1074/jbc.C111.328559.
34. **Zhou X, Yang W, Li J.** 2006. Ca2+- and protein kinase C-dependent signaling pathway for nuclear factor-kappaB activation, inducible nitric-oxide synthase expression, and tumor necrosis factor-alpha production in lipopolysaccharide-stimulated rat peritoneal macrophages. J Biol Chem **281:**31337–31347. http://dx.doi.org/10.1074/jbc.M602739200.
35. **Sundivakkam PC, Kwiatek AM, Sharma TT, Minshall RD, Malik AB, Tiruppathi C.** 2009. Caveolin-1 scaffold domain interacts with TRPC1 and IP3R3 to regulate Ca2+ store release-induced Ca2+ entry in endothelial cells. Am J Physiol Cell Physiol **296:**C403–C413. http://dx.doi.org/10.1152/ajpcell.00470.2008.
36. **Paria BC, Bair AM, Xue J, Yu Y, Malik AB, Tiruppathi C.** 2006. Ca2+ influx induced by protease-activated receptor-1 activates a feed-forward mechanism of TRPC1 expression via nuclear factor-kappaB activation in endothelial cells. J Biol Chem **281:**20715–20727. http://dx.doi.org/10.1074/jbc.M600722200.
37. **Yildirim E, Carey MA, Card JW, Dietrich A, Flake GP, Zhang Y, Bradbury JA, Rebolloso Y, Germolec DR, Morgan DL, Zeldin DC, Birnbaumer L.** 2012. Severely blunted allergen-induced pulmonary Th2 cell response and lung hyperresponsiveness in type 1 transient receptor potential channel-deficient mice. Am J Physiol Lung Cell Mol Physiol **303:**L539–L549. http://dx.doi.org/10.1152/ajplung.00389.2011.
38. **Ozaki T, Maeda M, Hayashi H, Nakamura Y, Moriguchi H, Kamei T, Yasuoka S, Ogura T.** 1989. Role of alveolar macrophages in the neutrophil-dependent defense system against Pseudomonas aeruginosa infection in the lower respiratory tract. Amplifying effect of muramyl dipeptide analog. Am Rev Respir Dis **140:**1595–1601.
39. **Wang J, Gigliotti F, Bhagwat SP, Maggirwar SB, Wright TW.** 2007. Pneumocystis stimulates MCP-1 production by alveolar epithelial cells through a JNK-dependent mechanism. Am J Physiol Lung Cell Mol Physiol **292:**L1495–L1505. http://dx.doi.org/10.1152/ajplung.00452.2006.
40. **Anderson P.** 2008. Post-transcriptional control of cytokine production. Nat Immunol **9:**353–359. http://dx.doi.org/10.1038/ni1584.
41. **Guma M, Stepniak D, Shaked H, Spehlmann ME, Shenouda S, Cheroutre H, Vicente-Suarez I, Eckmann L, Kagnoff MF, Karin M.** 2011. Constitutive intestinal NF-kappaB does not trigger destructive inflammation unless accompanied by MAPK activation. J Exp Med **208:**1889–1900. http://dx.doi.org/10.1084/jem.20110242.
42. **Albert AP, Large WA.** 2002. Activation of store-operated channels by noradrenaline via protein kinase C in rabbit portal vein myocytes. J Physiol **544:**113–125. http://dx.doi.org/10.1113/jphysiol.2002.022574.
43. **Vanden Abeele F, Shuba Y, Roudbaraki M, Lemonnier L, Vanoverberghe K, Mariot P, Skryma R, Prevarskaya N.** 2003. Store-operated Ca2+ channels in prostate cancer epithelial cells: function, regulation, and role in carcinogenesis. Cell Calcium **33:**357–373. http://dx.doi.org/10.1016/S0143-4160(03)00049-6.
44. **Meseguer V, Alpizar YA, Luis E, Tajada S, Denlinger B, Fajardo O, Manenschijn JA, Fernandez-Pena C, Talavera A, Kichko T, Navia B, Sanchez A, Senaris R, Reeh P, Perez-Garcia MT, Lopez-Lopez JR, Voets T, Belmonte C, Talavera K, Viana F.** 2014. TRPA1 channels mediate acute neurogenic inflammation and pain produced by bacterial endotoxins. Nat Commun **5:**3125. http://dx.doi.org/10.1038/ncomms4125.
45. **Ahmmed GU, Mehta D, Vogel S, Holinstat M, Paria BC, Tiruppathi C, Malik AB.** 2004. Protein kinase Calpha phosphorylates the TRPC1 channel and regulates store-operated Ca2+ entry in endothelial cells. J Biol Chem **279:**20941–20949. http://dx.doi.org/10.1074/jbc.M313975200.

TRPC1 deficiency impairs host defense and proinflammatory responses to bacterial infection by regulating PKCα signaling

Xikun Zhou[1,2†], Yan Ye[2†], Yuyang Sun[2†], Xuefeng Li[1,2], Wenxue Wang[2], Breanna Privratsky[2], , Shirui Tan[2], Zongguang Zhou[3], Canhua Huang[1], Yu-quan Wei[1], Lutz Birnbaumer[4], Brij B. Singh[2*] and Min Wu[2*]

SUPPLEMENTARY FIGURES LEGENDS

Figure S1. Increased bacterial invasion and decreased PMN infiltration in TRPC1$^{-/-}$ mice. (A and B) *In vivo* imaging of bacterial infected mice (n=5). TRPC1$^{-/-}$ mice and WT mice were intranasally challenged with 1×10^7 CFU/mouse of Xen-41 (a bioluminescent strain of *P. aeruginosa*). Then the mice were monitored up to 24 h. (A) Images showing bioluminescence in the lung at different time points were obtained using IVIS XRII system. (B) The lungs of WT and TRPC1$^{-/-}$ mice were taken images with IVIS XRII system at 24 h. (C) Mice were infected with 1×10^7 CFU of PAO1 and sacrificed at 24 h post-infection (n=5). Lung and serum were aseptically collected to evaluate PMN infiltration. PMN cell percentages in the lung and serum were calculated versus total nuclear cells via HEMA-3 staining. Data are shown as means ± SDEVs and representative of three experiments (*p<0.05 by Student's t test).

Figure S2. Validation of the function of AMs. (A) TRPC1$^{-/-}$ and WT mice were irradiated (800rds) and administered antibiotics via treated drinking water (using 250 units/ml penicillin and 250 μg/ml Streptomycin). 10 million bone marrow cells from donor mice were injected into each recipient mouse via *i.v.* immediately after the isolation. 45 days later, these mice were challenged with Pa infection (n= 6 in each set of animals). BAL fluid was collected at 24

h and AMs in the precipitate were lysed. The colony formation units in the same number of AMs were calculated. (B) Same amounts of AM cells isolated from the TRPC1$^{-/-}$ and WT mice (n=5) were infected with PAO1-GFP at MOI 10:1 for 1 h. Fluorescence intensity showed decreased phagocytosis in TRPC1$^{-/-}$ mice. (C, D) Ca^{2+} imaging was performed in the presence of thapsigargin (2 μM) in various conditions in primary alveolar macrophages (AM) cells from (A). Analog plots of the fluorescence ratio (340/380) from an average of 40-60 cells are shown and been quantified. Data in was plotted as means ± SDEVs calculated by One-Way ANOVA with Tukey's post-hoc; (*p<0.05). All *in vitro* experiments were performed at least three times with similar results.

Figure S3. Verification of the function of siRNAs and **Ca^{2+} currents.** (A-B) MLE-12 cells were transfected with scrambled, TRPC1, or PKCα siRNA at 50 nM. Protein lysates prepared 24 h post-transfection were analyzed for (A) TRPC1 and (B) PKCα expression by western blotting. GAPDH serves as the loading control. (C) Ca^{2+} imaging was performed in the presence of Tg (1μM) on MLE-12 cell. Analog plots of the fluorescence ratio (340/380) from an average of 40-60 cells are shown and been quantified (shown as bar graph in D). (E) Basal control of Ca^{2+} imaging was performed in the presence of Pa on MLE-12 cell.

Figure S4. Bacterial infection facilitated Ca2^{+} influx. (A) Ca^{2+} imaging was performed in the presence of LPS (100 ng/ml) in scrambled siRNA and TRPC1 siRNA transfected MLE-12 cells. Analog plots and quantification of the fluorescence ratio (340/380) from an average of 40-60 cells are shown. (B and C) LPS-induced currents were evaluated in scrambled and TRPC1 siRNA transfected MLE-12 cells with the holding potential at -80mV (B).

Representative IV curves under these conditions and the average (8-10 recordings) current intensity under various conditions are shown in (D). (E) MLE-12 cells were transfected with scrambled siRNA, STIM1 siRNA for 48 h and Ca^{2+} imaging was performed in the presence of LPS (100 ng/ml) in control, siSTIM1 MLE-12 cells. Analog plots of the fluorescence ratio (340/380) from an average of 40-60 cells' peak values are shown and been quantified in (F). Western blots showing decreased expression of STIM1 using siRNAs are shown in inset. Ca^{2+} imaging was performed in the presence of OAG (100 μM) in control and Pa-treated (15min and 30min) MLE-12 cells. Analog plots of the fluorescence ratio (340/380) from an average of 40-60 cells are shown after quantification. Data in (A, C, D) were plotted as means ± SDEVs calculated by Student's *t* test (A, C) or One-Way ANOVA with Tukey's post-hoc (D); (*p<0.05). All experiments were performed at least three times with similar results.

Figure S5. Densitometric quantification of the western blotting gel data presented in Fig. 3 using Quantity One software. (A) Densitometric quantification of the western blotting gel data presented in Fig. 3A. (B) Densitometric quantification of the western blotting gel data presented in Fig. 3C. (C) Densitometric quantification of the western blotting gel data presented in Fig. 3G.

Figure S6. The expression trend of TLRs-relevant genes. WT mice were intranasally infected with 1×10^7 CFU/mouse of PAO1 for different time points. Lung tissues were lysed to assess the levels of various signaling proteins. p-JNK, JNK, p-NF-κB p65 (Ser536), NF-κB p65, TNF-α and IL-6 levels were determined by western blotting. GAPDH serves as the loading control. Densitometric quantification of the western blotting gel data was used by

Quantity One software. The data are representative of three experiments.

Figure S7. Elevated activation of NF-κB induced upon bacterial infection in MLE-12 cells. (A) The translocation of p-JNK and p-NF-κB p65 after PAO1 infection using immune staining. Cells were pre-treated with 20 μM JNK inhibitor SP600125 and 50 μg/ml NF-κB inhibitor SN50 for 30 min before infection. DAPI was used to stain the nucleus. (B) Activation of NF-κB was detected using a luciferase promoter assay. Transient transfections were performed 24 h before infection. PAO1 infection at 10:1 MOI for 1 h and cell lysates were subjected to luciferase activity analysis using the Dual-Luciferase Reporter Assay System. The data are representative of three experiments (*p<0.05). Average values and SDEVs were calculated by One-Way ANOVA with Tukey's post-hoc. The data are representative of three experiments.

Figure S8. Densitometric quantification of the western blotting gel data presented in Fig. 4 using Quantity One software. (A) Densitometric quantification of the western blotting gel data presented in Fig. 4A. (B) Densitometric quantification of the western blotting gel data presented in Fig. 4B. (C) Densitometric quantification of the western blotting gel data presented in Fig. 4C.

Figure S9. TRPC1 has similar function in host defense against K. pneumoniae and PAK infection. MH-S cells were transfected with scrambled or TRPC1, or PKCα siRNA (50 nM) for 24 h. Then the cells were infected with Kp or PAK (another Pa strain with more cellular toxicity to validate the PAO1 data as a comparison) at MOI 10:1 for 1 h and polymyxin B (100

μg/ml) was added into the medium for another indicated time. Different cytokines in the supernatant of MH-S cells were measured by a standard ELISA 16 h after bacterial infection. Data are plotted as means ± SDEVs calculated by One-Way ANOVA with Tukey's post-hoc. (*p<0.05). All experiments were performed at least three times with similar results.

Figure S10. Densitometric quantification of the western blotting gel data presented in Fig. 5 using Quantity One software. (A) Densitometric quantification of the western blotting gel data presented in Fig. 5A. (B) Densitometric quantification of the western blotting gel data presented in Fig. 5B. (C) Densitometric quantification of the western blotting gel data presented in Fig. 5E.

Figure S11. TLR4 mediated signaling facilitated $Ca2^+$ influx. (A) Ca^{2+} imaging was performed in the presence of LPS in scrambled and MyD88 siRNA transfected MH-S cells. Quantification of fluorescence ratio (340/380) from an average of 100-125 under various conditions infected with PAO1 is shown. (B) Representative IV curves under the treatment of the TLR4 inhibitor, E5564, infected with PAO1 in MH-S cells and the average (8-10 recordings) current intensity (at -80mV) in control and Pa-treated are shown. (C) Representative IV curves and the average (8-10 recordings) current intensity (at -80mV) in E55564 treated MH-S cells in the persistence of additional IP_3. Data in (A-D) were plotted as means ± SDEVs calculated by One-Way ANOVA with Tukey's post-hoc (A, and D) or Student's t test (B-C); (*p<0.05). All experiments were performed at least three times with similar results.

Figure S1.

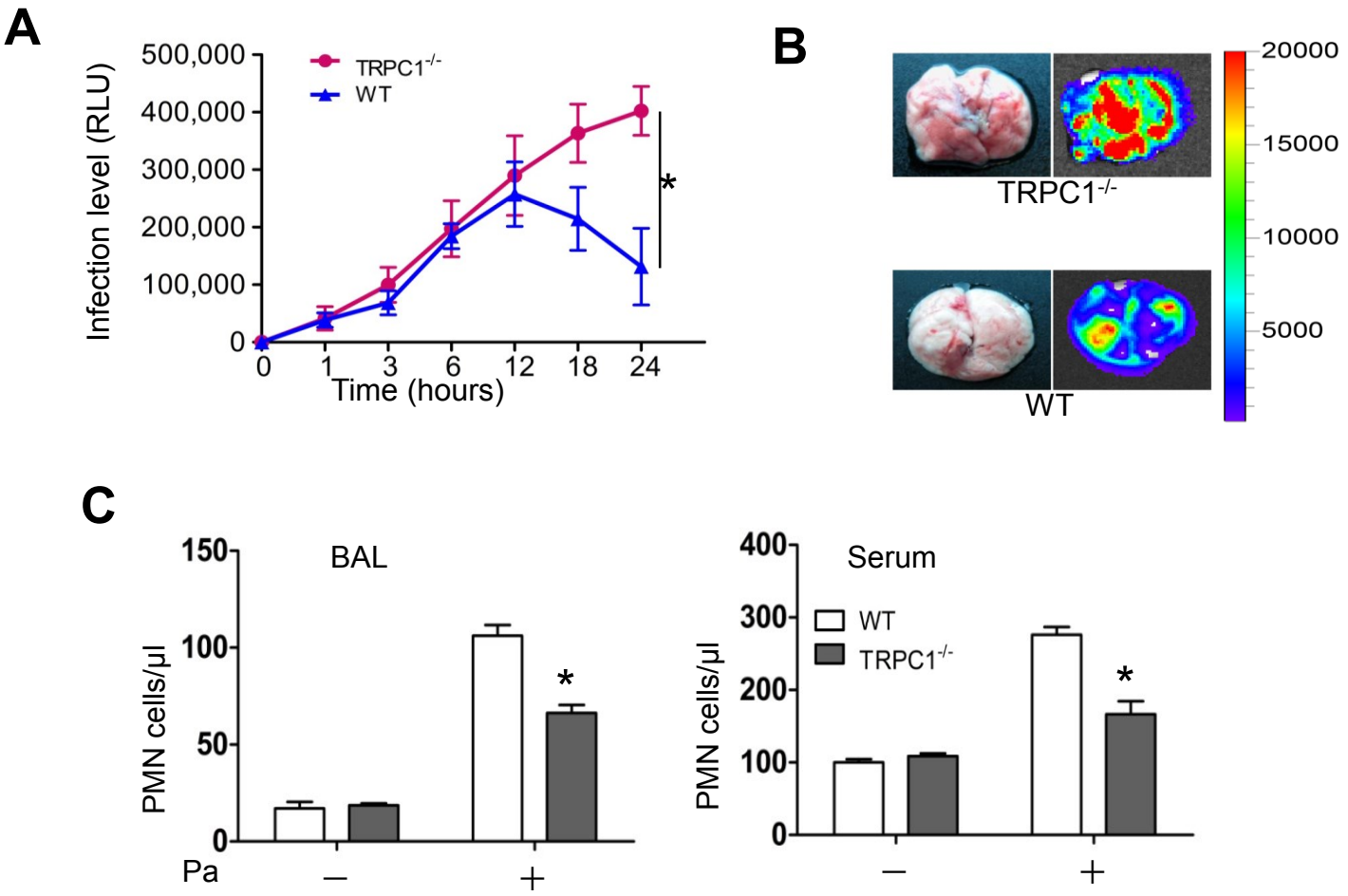
A
Infection level (RLU)
500,000
400,000
300,000
200,000
100,000
0
TRPC1-/-
WT
*
0
1
3
6
12
18
24
Time (hours)
B
TRPC1-/-
WT
20000
15000
10000
5000
C
BAL
PMN cells/µl
150
100
50
0
*
Pa
–
+
Serum
400
300
200
100
0
WT
TRPC1-/-
*
–
+

Figure S2.

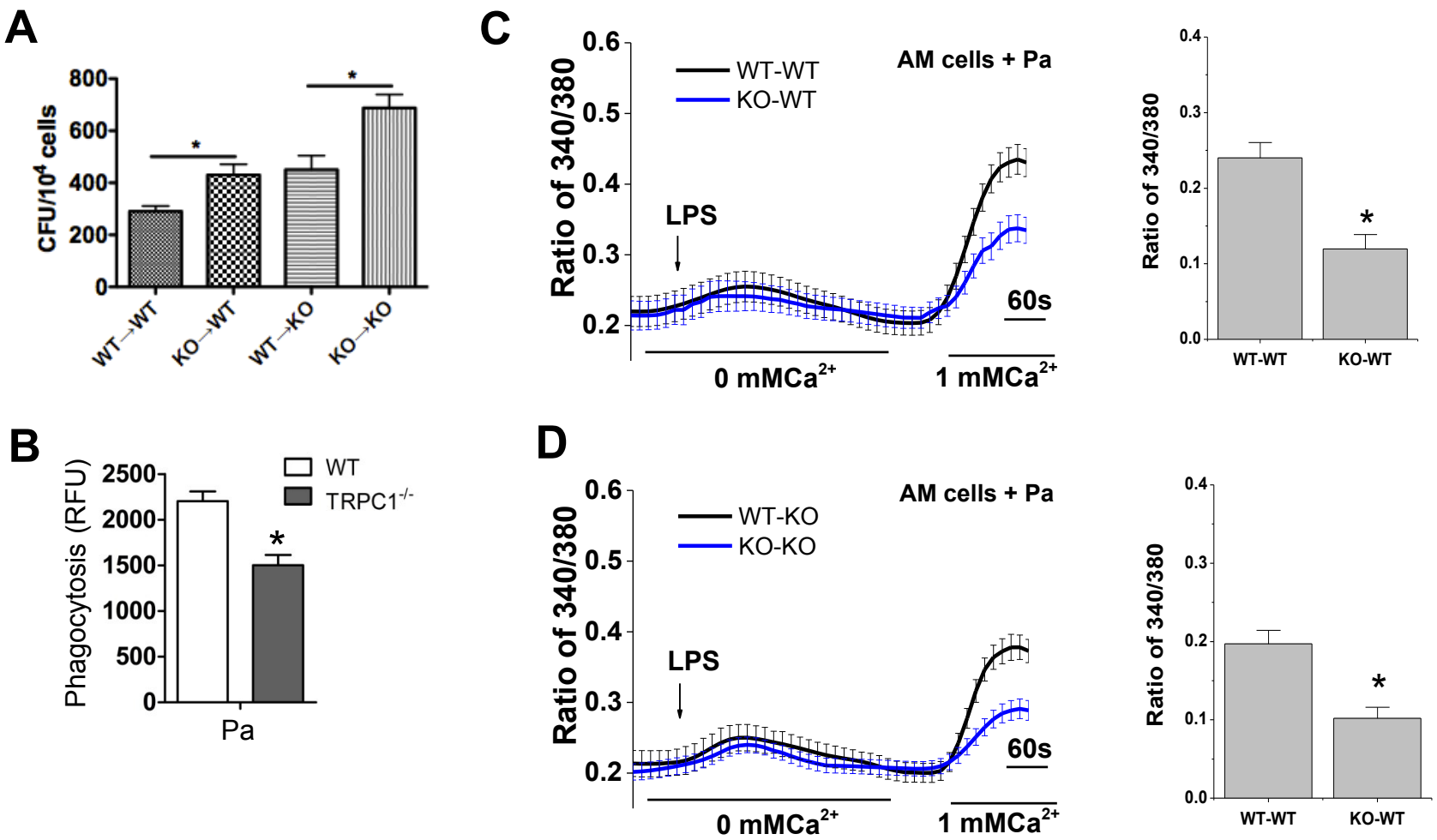
A
CFU/10^4 cells
800
600
400
200
0
*
*
WT→WT
KO→WT
WT→KO
KO→KO
B
Phagocytosis (RFU)
2500
2000
1500
1000
500
0
WT
TRPC1-/-
*
Pa
C
Ratio of 340/380
0.6
0.5
0.4
0.3
0.2
WT-WT
KO-WT
AM cells + Pa
LPS
60s
0 mMCa2+
1 mMCa2+
Ratio of 340/380
0.4
0.3
0.2
0.1
0.0
*
WT-WT
KO-WT
D
Ratio of 340/380
0.6
0.5
0.4
0.3
0.2
WT-KO
KO-KO
AM cells + Pa
LPS
60s
0 mMCa2+
1 mMCa2+
Ratio of 340/380
0.4
0.3
0.2
0.1
0.0
*
WT-WT
KO-WT

Figure S3.

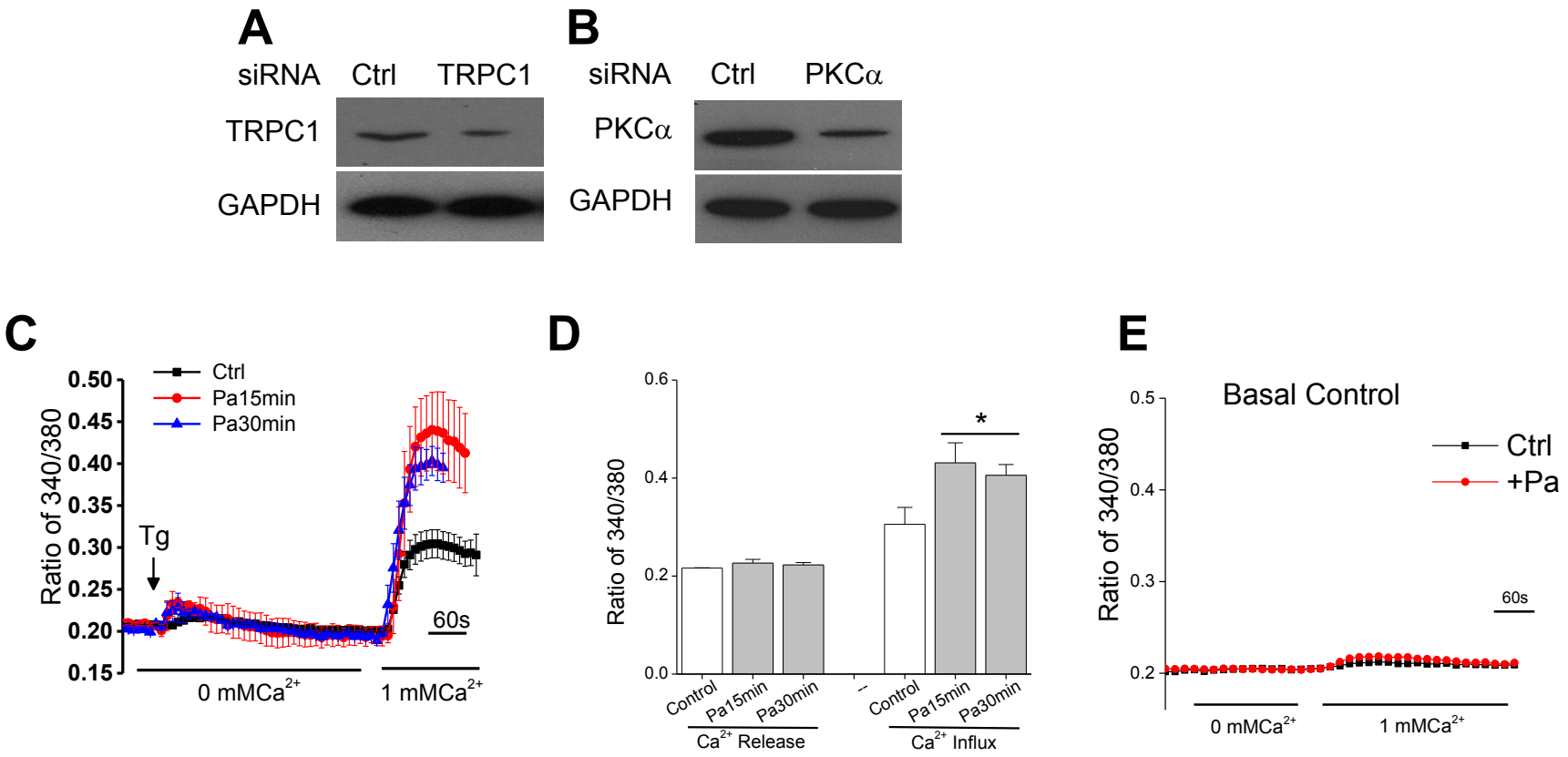
A
siRNA
Ctrl
TRPC1
TRPC1
GAPDH
B
siRNA
Ctrl
PKCα
PKCα
GAPDH
C
Ctrl
Pa15min
Pa30min
Ratio of 340/380
0.50
0.45
0.40
0.35
0.30
0.25
0.20
0.15
Tg
60s
0 mMCa2+
1 mMCa2+
D
Ratio of 340/380
0.6
0.4
0.2
0.0
*
Control
Pa15min
Pa30min
Control
Pa15min
Pa30min
Ca2+ Release
Ca2+ Influx
E
Basal Control
Ctrl
+Pa
Ratio of 340/380
0.5
0.4
0.3
0.2
60s
0 mMCa2+
1 mMCa2+

Figure S4.

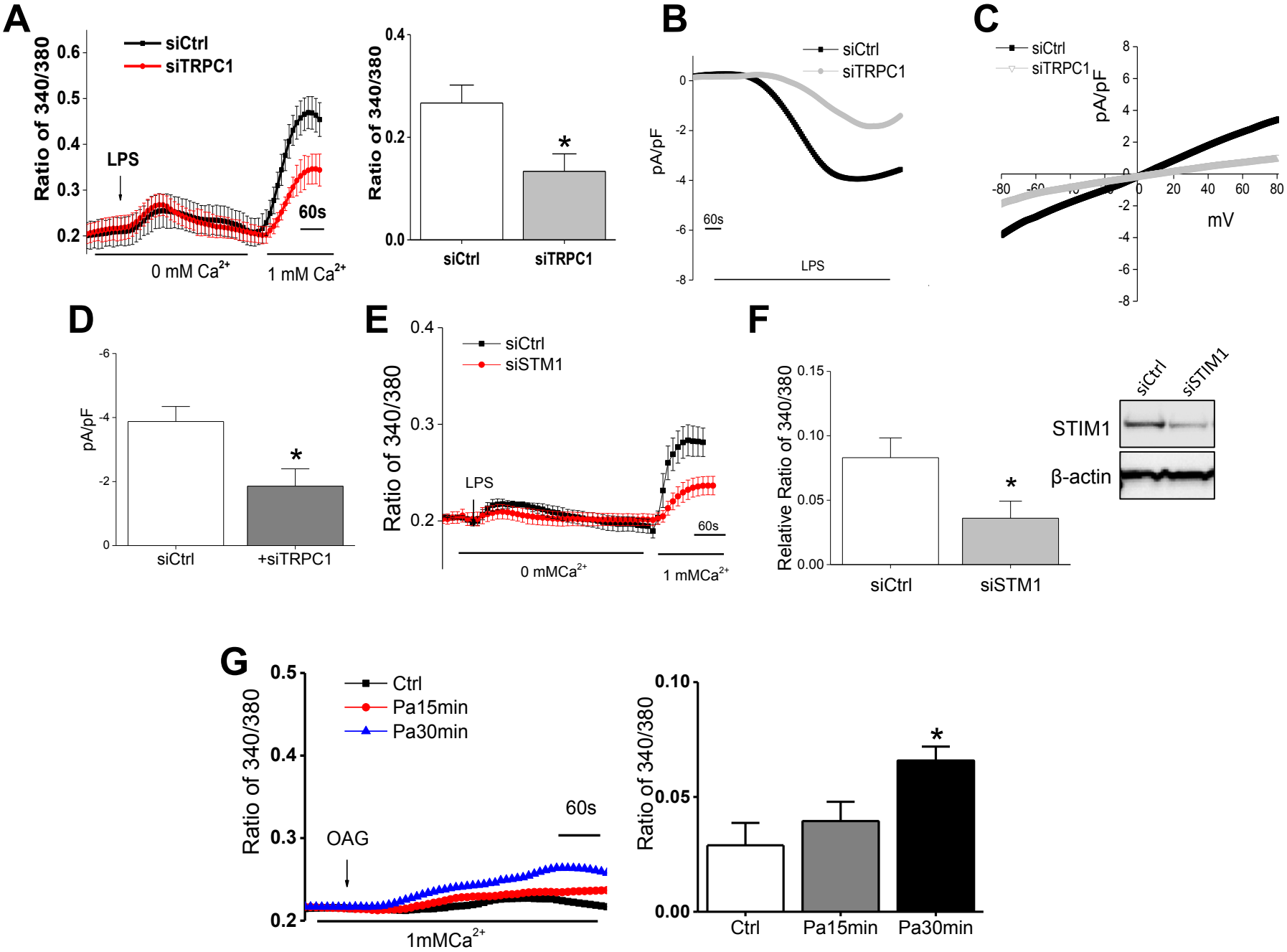
A
siCtrl
siTRPC1
Ratio of 340/380
LPS
60s
0 mM Ca2+
1 mM Ca2+
siCtrl
siTRPC1
B
siCtrl
siTRPC1
pA/pF
60s
LPS
C
siCtrl
siTRPC1
pA/pF
mV
D
pA/pF
siCtrl
+siTRPC1
E
siCtrl
siSTM1
Ratio of 340/380
LPS
60s
0 mMCa2+
1 mMCa2+
F
Relative Ratio of 340/380
siCtrl
siSTIM1
siCtrl
siSTIM1
STIM1
β-actin
G
Ctrl
Pa15min
Pa30min
Ratio of 340/380
OAG
60s
1mMCa2+
Ratio of 340/380
Ctrl
Pa15min
Pa30min

Figure S5.

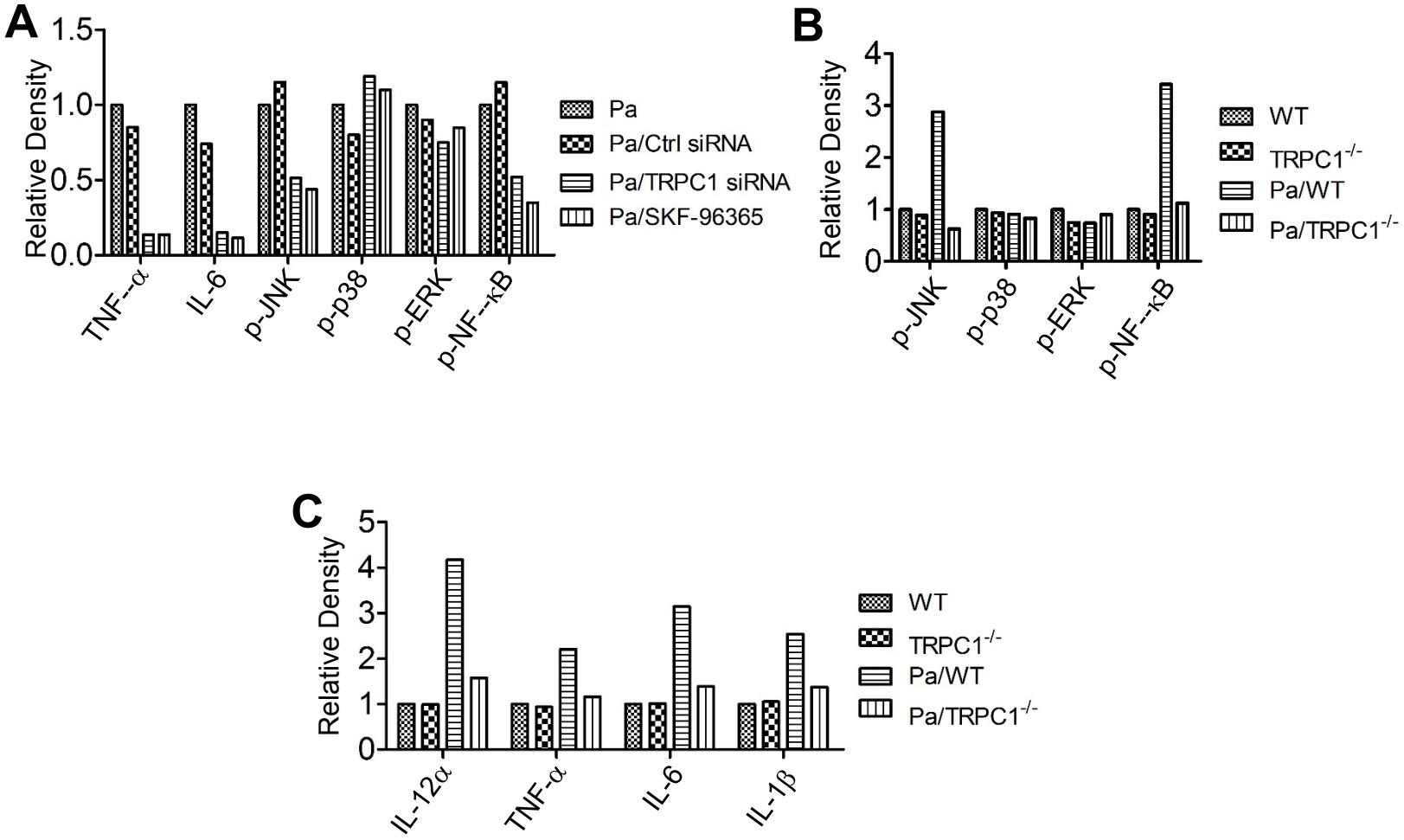
A
Relative Density
1.5
1.0
0.5
0.0
TNF-α
IL-6
p-JNK
p-p38
p-ERK
p-NF-κB
Pa
Pa/Ctrl siRNA
Pa/TRPC1 siRNA
Pa/SKF-96365
B
Relative Density
4
3
2
1
0
p-JNK
p-p38
p-ERK
p-NF-κB
WT
TRPC1-/-
Pa/WT
Pa/TRPC1-/-
C
Relative Density
5
4
3
2
1
0
IL-12α
TNF-α
IL-6
IL-1β
WT
TRPC1-/-
Pa/WT
Pa/TRPC1-/-

Figure S6.

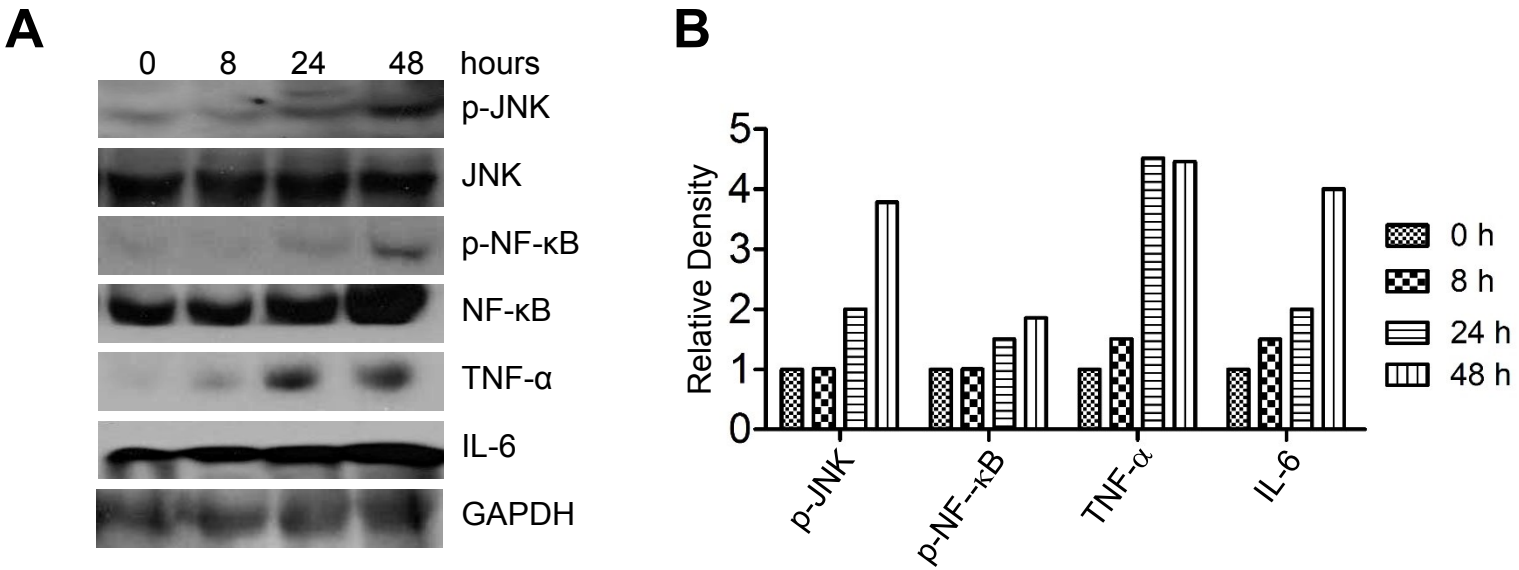
A
0
8
24
48
hours
p-JNK
JNK
p-NF-κB
NF-κB
TNF-α
IL-6
GAPDH
B
Relative Density
0
1
2
3
4
5
p-JNK
p-NF-κB
TNF-α
IL-6
0 h
8 h
24 h
48 h

Figure S7.

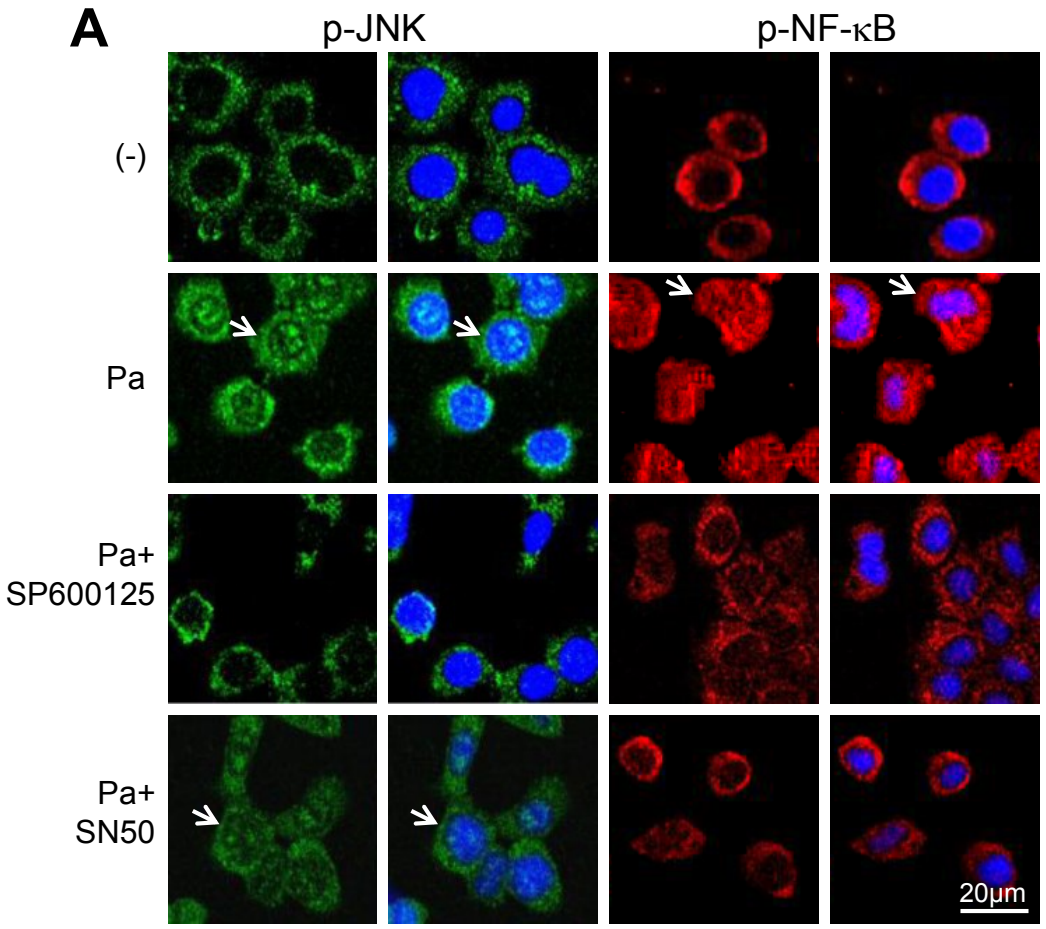
A
p-JNK
p-NF-κB
(-)
Pa
Pa+
SP600125
Pa+
SN50
20μm

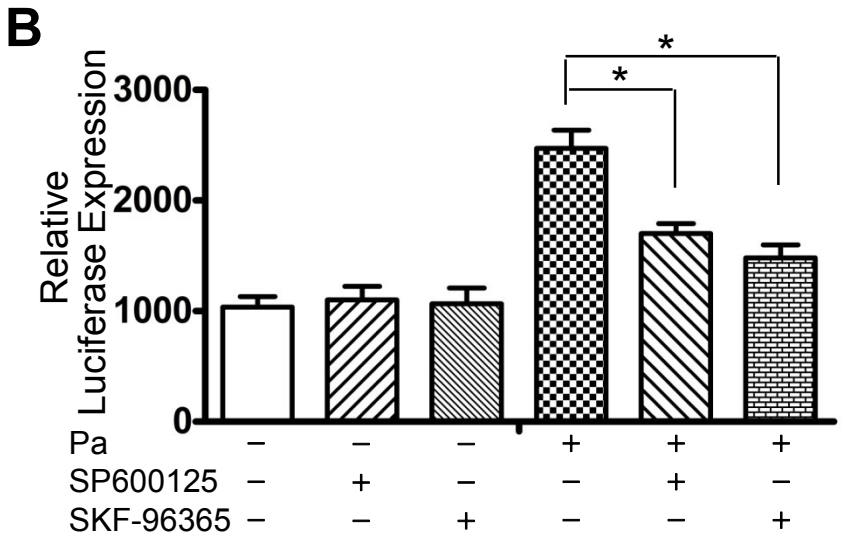
B
Relative Luciferase Expression
3000
2000
1000
0
*
*
Pa – – – + + +
SP600125 – + – – + –
SKF-96365 – – + – – +

Figure S8.

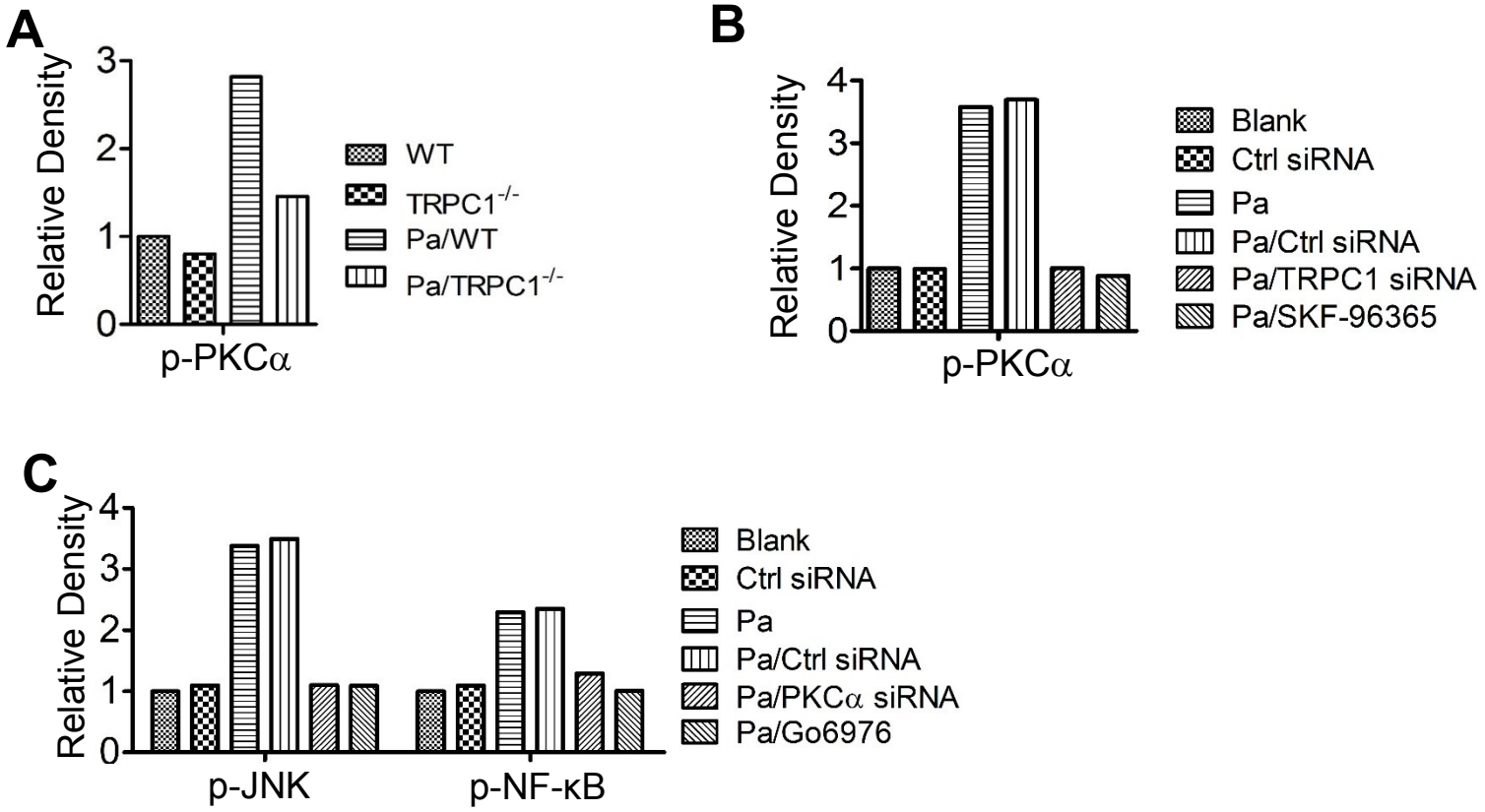
A
Relative Density
3
2
1
0
p-PKCα
WT
TRPC1-/-
Pa/WT
Pa/TRPC1-/-
B
Relative Density
4
3
2
1
0
p-PKCα
Blank
Ctrl siRNA
Pa
Pa/Ctrl siRNA
Pa/TRPC1 siRNA
Pa/SKF-96365
C
Relative Density
4
3
2
1
0
p-JNK
p-NF-κB
Blank
Ctrl siRNA
Pa
Pa/Ctrl siRNA
Pa/PKCα siRNA
Pa/Go6976

Figure S9.

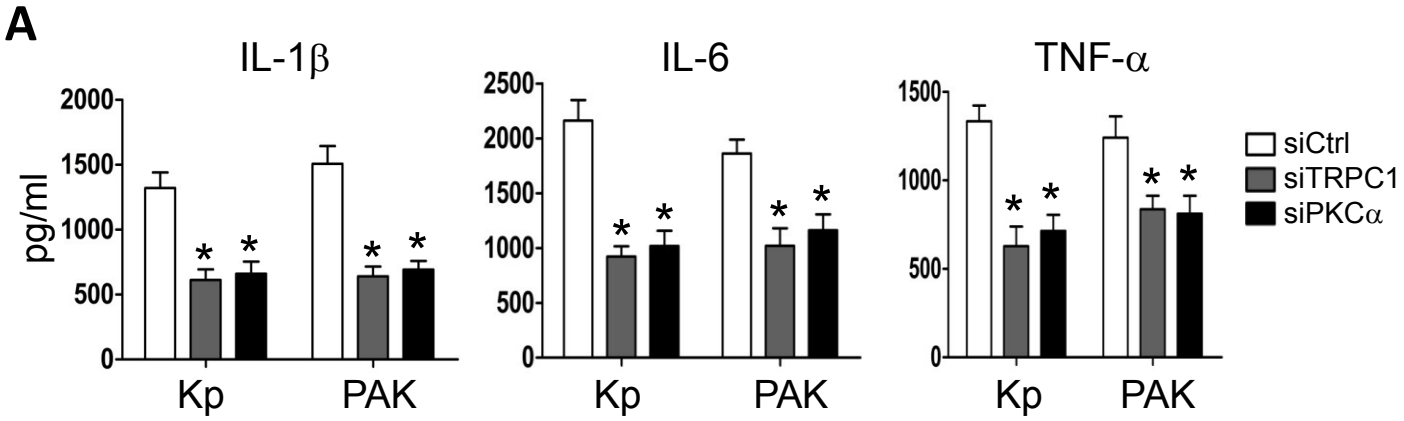
A
IL-1β
IL-6
TNF-α
pg/ml
2000
1500
1000
500
0
2500
2000
1500
1000
500
0
1500
1000
500
0
Kp
PAK
Kp
PAK
Kp
PAK
siCtrl
siTRPC1
siPKCα
*

Figure S10.

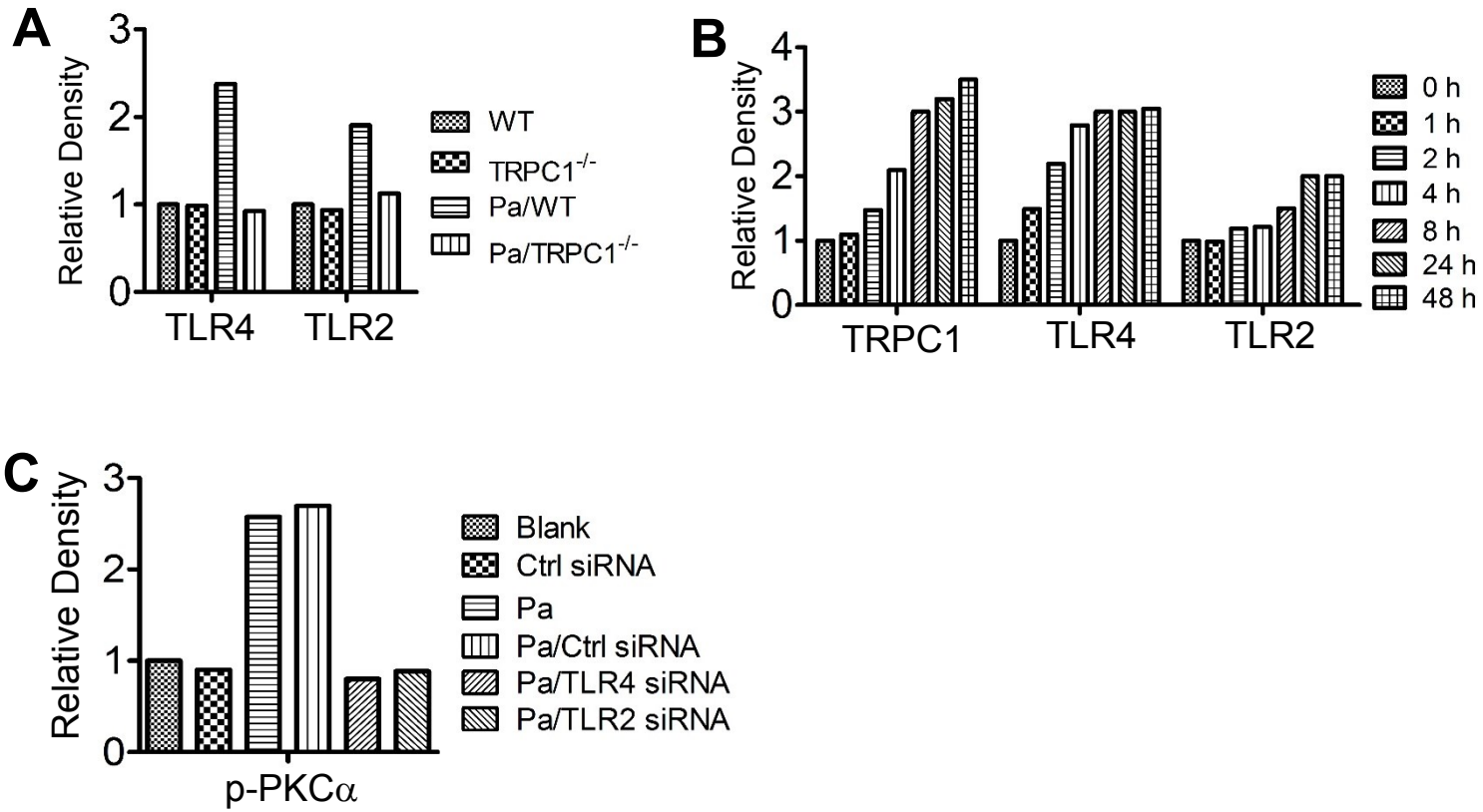
A
Relative Density
3
2
1
0
TLR4
TLR2
WT
TRPC1-/-
Pa/WT
Pa/TRPC1-/-
B
Relative Density
4
3
2
1
0
TRPC1
TLR4
TLR2
0 h
1 h
2 h
4 h
8 h
24 h
48 h
C
Relative Density
3
2
1
0
p-PKCα
Blank
Ctrl siRNA
Pa
Pa/Ctrl siRNA
Pa/TLR4 siRNA
Pa/TLR2 siRNA

Figure S11.

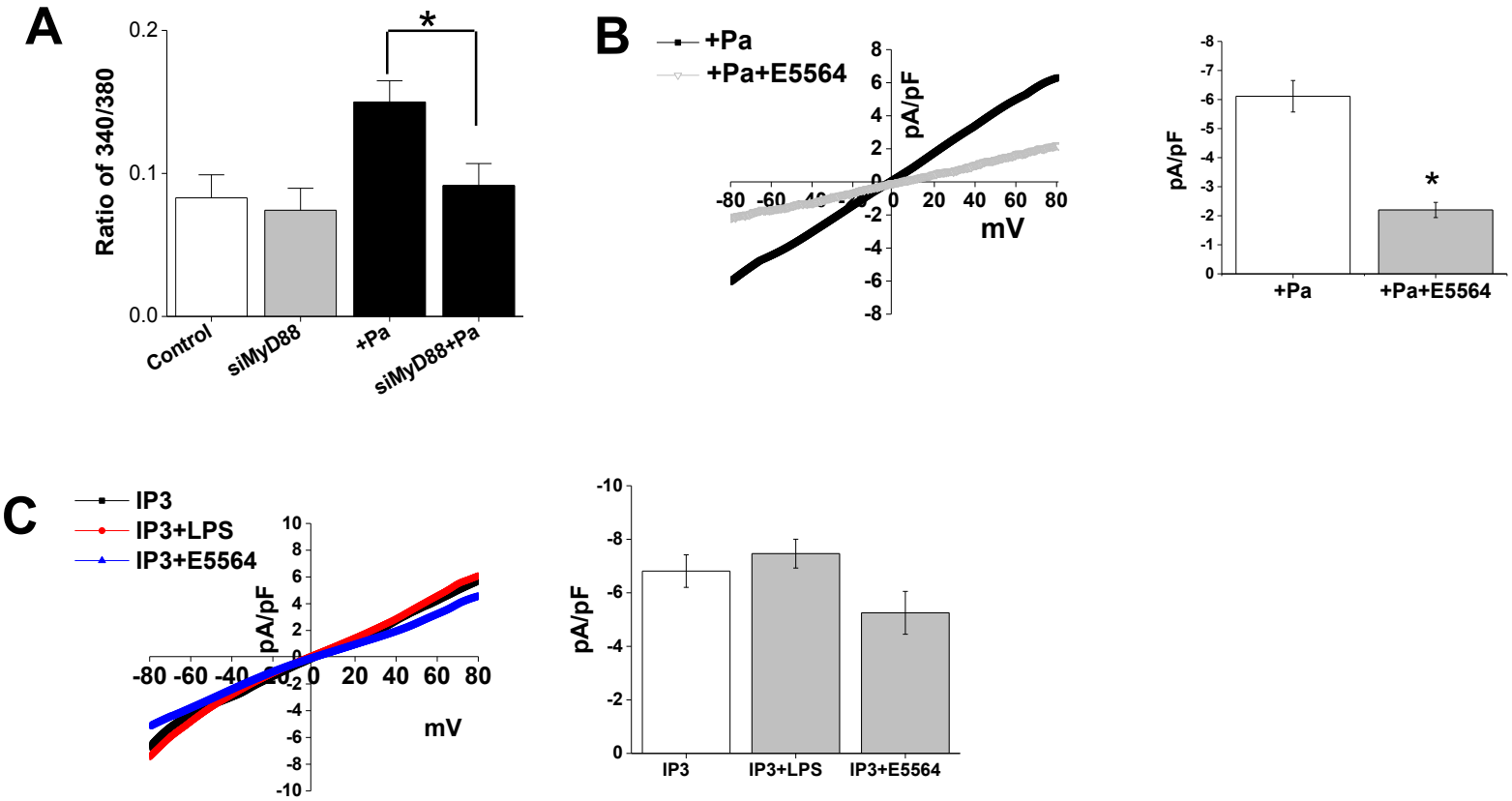
A
Ratio of 340/380
0.2
0.1
0.0
*
Control
siMyD88
+Pa
siMyD88+Pa
B
+Pa
+Pa+E5564
pA/pF
mV
pA/pF
*
+Pa
+Pa+E5564
C
IP3
IP3+LPS
IP3+E5564
pA/pF
mV
pA/pF
IP3
IP3+LPS
IP3+E5564